

---

Electronic Thesis and Dissertation Repository

---

7-26-2016 12:00 AM

## Hybrid Magneto-Rheological Actuators for Human Friendly Robotic Manipulators

Masoud Moghani  
*The University of Western Ontario*

Supervisor  
Dr. Mehrdad R. Kermani  
*The University of Western Ontario*

Graduate Program in Electrical and Computer Engineering  
A thesis submitted in partial fulfillment of the requirements for the degree in Master of Engineering Science  
© Masoud Moghani 2016

Follow this and additional works at: <https://ir.lib.uwo.ca/etd>



Part of the [Controls and Control Theory Commons](#), and the [Electro-Mechanical Systems Commons](#)

---

### Recommended Citation

Moghani, Masoud, "Hybrid Magneto-Rheological Actuators for Human Friendly Robotic Manipulators" (2016). *Electronic Thesis and Dissertation Repository*. 3907.  
<https://ir.lib.uwo.ca/etd/3907>

This Dissertation/Thesis is brought to you for free and open access by Scholarship@Western. It has been accepted for inclusion in Electronic Thesis and Dissertation Repository by an authorized administrator of Scholarship@Western. For more information, please contact [wlsadmin@uwo.ca](mailto:wlsadmin@uwo.ca).

# Abstract

In recent years, many developments in the field of the physical human robot interaction (pHRI) have been witnessed and significant attentions have been given to the subject of safety within the interactive environments. Ensuring the safety has led to the design of the robots that are physically unable to hurt humans. However, Such systems commonly suffer from the safety-performance trade-off. Magneto-Rheological (MR) fluids are a special class of fluids that exhibit variable yield stress with respect to an applied magnetic field. Devices developed with such fluids are known to provide the prerequisite requirements of intrinsic safe actuation while maintaining the dynamical performance of the actuator.

In this study, a new concept for generating magnetic field in Magneto-Rheological (MR) clutches is presented. The main rationale behind this concept is to divide the magnetic field generation into two parts using an electromagnetic coil and a permanent magnet. The main rationale behind this concept is to utilize a hybrid combination of electromagnetic coil and a permanent magnet. The combination of permanent magnets and electromagnetic coils in Hybrid Magneto-Rheological (HMR) clutches allows to distribute the magnetic field inside an MR clutch more uniformly. Moreover, The use of a permanent magnet dramatically reduces the mass of MR clutches for a given value of the nominal torque that results in developing higher torque-to-mass ratio. High torque-to-mass and torque-to-inertia ratios in HMR clutches promotes the use of these devices in human-friendly actuation.

**Keywords:** Human Friendly Robots, Magneto-Rheological Actuator, MR Clutch, Hybrid Magneto-Rheological Actuator, HMR Actuator, Intrinsically Safe Actuators, Soft Robotics.

## Co-Authorship Statement

This thesis is written by Masoud Moghani, and reviewed and edited by Dr. Mehrdad R. Kermani. Parts of this material were published in peer-reviewed conference proceedings.

Chapter 2:

Moghani M., Kermani, M. R., “Design and Development of a Hybrid Magneto-Rheological Clutch for Safe Robotic Applications,” In 2016 IEEE International Conference on Robotics and Automation (ICRA), Stockholm, Sweden

Chapter 4:

Moghani M., Kermani M. R., “Hysteresis Modeling of a Hybrid Magneto- Rheological Actuator,” in 2016 IEEE International Conference on Advanced Intelligent Mechatronics, Banff, Alberta, Canada

## Acknowledgements

I express my gratitude to my supervisor Dr. Mehrdad Kermani for giving me the opportunity to be part of his research team and to entrust me with this project. I owe special thanks to him for sharing with me his comprehensive expertise in actuators and robotics.

I would like to thank my parents for their unlimited support during my studies. I did the most important part of my studies without being beside them. But my loving mother, she never forgot to call or text me Good morning! every single day.

Finally, I would also like to thank my lab-mates, specially Dr. Peyman Yadmellat, Mahyar Abdeetedal, and Wenjun Li for sharing their experience and knowledge with me.

*To pieces of my heart, my parents: Esrafil and Khadijeh,  
my two lovely sisters: Afsaneh and Farzaneh.*

# Contents

<b>Abstract</b>	<b>ii</b>
<b>Co-Authorship Statement</b>	<b>iii</b>
<b>Acknowledgements</b>	<b>iv</b>
<b>List of Figures</b>	<b>x</b>
<b>List of Tables</b>	<b>xiii</b>
<b>1 Introduction</b>	<b>1</b>
1.1 Review of Human-Safe Robots and Human-Friendly Actuation . . . . .	2
1.1.1 Safeguarding and Collision Avoidance . . . . .	2
1.1.2 Light Weight Manipulators and Robots . . . . .	2
1.1.3 Complaint Actuators . . . . .	3
1.1.4 Variable Damper Actuators . . . . .	4
1.1.5 Distributed Active Semi-Active Actuation Approach . . . . .	4
1.2 Magneto-Rheological Devices and Actuators . . . . .	5
1.2.1 MR Fluid Durability . . . . .	5
Hard cake . . . . .	6
Clumping effects . . . . .	6
Particles oxidation . . . . .	6
1.2.2 MR Fluid Characteristic . . . . .	6
1.3 Objectives . . . . .	7
1.3.1 Contributions . . . . .	9
Introduction of a Hybrid MR Actuator . . . . .	9

Development of a Hybrid MR Actuator . . . . .	9
Modeling Hysteresis in MR Actuators . . . . .	9
1.3.2 Thesis Outline . . . . .	10
<b>Bibliography</b>	<b>10</b>
<b>2 Design and Development of a Hybrid Magneto-Rheological Actuator</b>	<b>16</b>
2.1 Introduction . . . . .	17
2.2 MR Actuator . . . . .	18
2.2.1 MR Clutch Modeling Using FEM . . . . .	20
2.3 MR Clutch Model Verification . . . . .	21
2.4 Permanent Magnet Based MR Clutch . . . . .	24
2.4.1 Material Selection . . . . .	24
2.4.2 Optimization . . . . .	26
2.4.3 Result Analysis . . . . .	29
2.5 Conclusions . . . . .	32
<b>Bibliography</b>	<b>32</b>
<b>3 Prototype Hybrid Magneto-Rheological Actuator</b>	<b>35</b>
3.1 Introduction . . . . .	35
3.2 Design and Development of Hybrid MR Clutch . . . . .	37
3.2.1 Hybrid MR Clutch . . . . .	37
3.2.2 Design Of a Hybrid MR Clutch . . . . .	39
3.2.3 Actuator Mass . . . . .	40
3.2.4 Finite Element Analysis and Optimization . . . . .	42
3.3 Prototype Hybrid MR clutch . . . . .	47
3.4 Experimental Validation of the Prototype Hybrid MR Clutch . . . . .	48
3.4.1 Experimental System . . . . .	48
3.4.2 Current vs. Torque . . . . .	49
Step Response . . . . .	49
Open-loop Frequency Response . . . . .	51
3.4.3 Torque Control Experiments . . . . .	51
Tracking of Desired Input . . . . .	53

Frequency Response . . . . .	53
3.4.4 Position Tracking Control Experiments . . . . .	54
A-DASA motion control . . . . .	54
Repeatability . . . . .	57
3.5 Conclusions . . . . .	57
<b>Bibliography</b>	<b>62</b>
<b>4 Hysteresis Modeling of a Hybrid Magneto-Rheological Actuator</b>	<b>65</b>
4.1 Introduction . . . . .	66
4.2 Hybrid MR Actuator . . . . .	68
4.2.1 Prototype Hybrid MR clutch . . . . .	68
4.2.2 Integration of the Magnetic Sensor . . . . .	70
4.3 Modeling and Control of Hybrid MR Actuator . . . . .	71
4.3.1 Artificial Neural network . . . . .	73
4.3.2 Torque Control Scheme . . . . .	74
4.4 Experimental Results . . . . .	76
4.4.1 Experimental Test Bench . . . . .	76
4.4.2 Validation of the Modeling Method . . . . .	76
4.4.3 Torque Control . . . . .	77
4.5 Conclusions and Future Works . . . . .	79
<b>Bibliography</b>	<b>79</b>
<b>5 Conclusions and Future Work</b>	<b>83</b>
5.1 Conclusion . . . . .	83
5.2 Future Work . . . . .	84
5.2.1 Validating Antagonistic DASA using HMR and Conventional MR clutches	84
5.2.2 Hybrid Motion-Force Control . . . . .	84
5.2.3 Multi-DOF Light Weight Manipulator . . . . .	84
5.2.4 Redesign the Location of the Hall Sensors . . . . .	85
<b>Bibliography</b>	<b>85</b>





# List of Figures

1.1	Yield Strength versus magnetic field strength of several typical MR fluids. . . .	7
1.2	Magnetic field versus magnetic field strength of several typical MR fluids. . . .	8
2.1	Cross-section of a multi-disk MR clutch. . . . .	20
2.2	The optimal designed MR clutch. . . . .	22
2.3	(a) Sinusoidal+DC component input current, (b) Output torque and magnetic flux density of the prototyped MR clutch. . . . .	23
2.4	Comparison between measured results and simulation. . . . .	23
2.5	Magnetic field distribution inside a hybrid MR clutch: (a) magnetic flux density (B field) distribution inside the MR clutch due to the permanent magnet (off-state), (b) the field enhancement in the MR clutch pack with an applied magnetic field, and (c) the field cancellation in the MR clutch pack due to an applied magnetic field in reverse direction. . . . .	25
2.6	Parameters and functional components of a hybrid MR clutch. . . . .	26
2.7	Torque-to-mass ratio vs. nominal torque. . . . .	28
2.8	Torque-to-mass ratio of a 6-disk hybrid MR clutch vs (a) cap (side disk) thickness, and (b) shaft diameter. . . . .	28
2.9	Magnetic flux density contour map in a conventional MR clutch. . . . .	30
2.10	Magnetic flux density contour map in a Hybrid MR clutch. . . . .	30
2.11	Preliminary results of the transient FEM analysis. Time evolution of the magnetic field at <i>time</i> = 0.05, 0.15, 0.30 (s) is shown in both conventional and hybrid MR clutches. . . . .	31
3.1	Cross-section of a hybrid MR clutch. . . . .	38
3.2	(a) Inner assembly of the clutch pack, (b) assembly of the HMR clutch. . . . .	41

3.3	Geometry of the HMR clutch and its design parameters. . . . .	42
3.4	A trade-off surface in three-dimensional objective space. . . . .	44
3.5	Magnetic flux density contour map in the Hybrid MR clutch when it is energized by (a) -2A, (b) 0A, (c) 2A, and (d) 4A. . . . .	45
3.6	Comparison between measured results and simulation. . . . .	46
3.7	Components of the prototype hybrid MR clutch. . . . .	47
3.8	Experimental test bench for testing the prototype hybrid MR clutch. . . . .	50
3.9	Block diagram of the frequency response experimentation. . . . .	50
3.10	Evaluation of the transient performance of the HMR clutch when it is subjected to an input current (a) 0 A to 1 A, (b) 0 A to -1 A. . . . .	52
3.11	Open-loop frequency response. . . . .	52
3.12	Closed-loop control block diagram . . . . .	53
3.13	Torque tracking with $T_d = \sin(2\pi t) + \sin(5 \times 2\pi t) + \sin(10 \times 2\pi t) + 15$ . . . . .	53
3.14	Closed loop frequency response of the prototyped HMR clutch. . . . .	54
3.15	Position tracking of sinusoidal input; period $T = 5$ sec. . . . .	55
3.16	Position tracking of sinusoidal input; period $T = 2.5$ sec. . . . .	56
3.17	A-DASA Position tracking result. . . . .	58
3.18	A-DASA Position tracking result. . . . .	59
3.19	Presence of external disturbance on A-DASA motion control. . . . .	60
3.20	Repeatability in force/torque control. . . . .	61
3.21	Repeatability in position control. . . . .	61
4.1	Magnetic field distribution inside a hybrid MR clutch: (a) magnetic flux density (B field) distribution inside the MR clutch due to the permanent magnet (off-state), (b) the field enhancement in the MR clutch pack with an applied magnetic field, and (c) the field cancellation in the MR clutch pack due to an applied magnetic field in reverse direction. . . . .	69
4.2	Prototype of the hybrid MR clutch. (a) Components of the prototype. (b) Assembly of the prototype. . . . .	70
4.3	Location of hall sensors inside the hybrid MR clutch. . . . .	72
4.4	Hysteretic behavior for an MR clutch. . . . .	72
4.5	Architecture of the feed-forward neural network. . . . .	74

4.6	Output torque versus magnetic field. . . . .	75
4.7	Closed-loop control configuration using embedded Hall sensors. . . . .	75
4.8	Experimental test bench. . . . .	76
4.9	Actual torque measurements versus estimations. . . . .	77
4.10	Torque control results for 1 Hz, 4 Hz, 6 Hz, and 8 Hz sinusoidal desired torque trajectories (from left to right). . . . .	78
4.11	Torque control results for multi-sinusoidal reference signal. . . . .	78
5.1	A-DASA Experimentation Platform. . . . .	85
5.2	Conceptual design of a light-weight robotic exoskeleton. . . . .	86
5.3	(a)Magnetic flux density contour map. (b)The path of the magnetic field is perpendicular to the surface of the Hall sensor. . . . .	86

# List of Tables

2.1	MR clutch specifications . . . . .	21
2.2	Optimization Variable . . . . .	27
2.3	Comparison of conventional and hybrid MR clutches . . . . .	32
3.1	Optimization Variable . . . . .	43
3.2	Configuration and properties of the permanent magnet . . . . .	48
3.3	Specifications of the hybrid MR clutch . . . . .	49
3.4	Comparison Between Prototype MR Clutches for Human-Friendly Actuator . .	51
4.1	Specifications of the Hybrid MR Clutch . . . . .	71

# Chapter 1

## Introduction

Roboticians have long foreseen humans and robots existing side by side and sharing work [1]. Since the 1960s, robotic systems have been developed and employed in different fields especially, automations and manufacturing industries. Robots have also been introduced into non-industrial areas such as homes and offices to help humans in living environment. However, there are several sources of danger when working closely with robotic devices. Unexpected collisions involving in collaboration of human and robot pose the highest degree of danger, mainly due to the unpredicted relative motion. Safeguarding systems were developed to insure the safety of the industrial robots. However, these methods are based on isolating human from robot workspace, and are not suitable in human-robot environments in which an interaction between the person and the robot is presupposed.

Safety in human-robot interaction has drawn large attention to development of intrinsically compliant robots which are able to suppress the impact forces caused by collision. The development of compliant actuators, however, has compromised dynamic performance. Subsequent evolutions increase mechanical complexities to maintain the dexterity of the actuation mechanism. In response to the increasing demand for human-safe robots, our research group introduced Distributed Active Semi-Active Actuation (DASA) approach. This actuation concept was originally disclosed in [2, 3]. DASA uses Magneto-Rheological (MR) clutches as its building block. MR clutches can produce large torques without gearing. These clutches offer high torque-to-mass and torque-to-inertia ratios, making them a proper candidate for human-friendly actuation. MR actuators are controlled by the intensity of the applied magnetic field. The aim of the current study is to introduce and analyse the use of parallel combination of

electromagnetic coil and permanent magnet in generating magnetic field inside an MR clutch.

## **1.1 Review of Human-Safe Robots and Human-Friendly Actuation**

### **1.1.1 Safeguarding and Collision Avoidance**

The use of safeguarding was a very first attempt to insure the safety of the industrial robots. The operation of the industrial robot is controlled by a separate robot controller in which prescribed instructions for accommodating the operation of the robot are preliminarily stored. However, it might occur that a movable part of the robot performs an erroneous movement while being programmed by an operator [4]. In order to prevent the occurrence of such erroneous movement of the robot, safeguard method such as locating a cage or fence around a robot, providing an emergency stop, limiting the movable range of the robot's part by means of hardware or software, etc., have been employed. However, these technologies prevent the human to be involved with robot in the area of the human-robot interaction.

Another approach is to hire sensors to prevent and detect collisions in robot applications. Such methods require knowledge of the robot's environment. Collision detection and avoidance in real time fashion are typically based on the use of additional external sensors, on-board vision [5], strain gauges [6], and torque/force sensors and load cells [7]. In the case of collision detection, the robot's controller should either stop the motion or perform an alternative task.

### **1.1.2 Light Weight Manipulators and Robots**

Light-weight robots are especially designed for mobility and interaction with a priori unknown environments and with humans. Whole-arm manipulation system (WAMS) is a cable-driven arm [8]. Tendon drive was used to achieve back-drivable speed reductions that increase the stiffness of the robotic structure, and also provide efficient, smooth, light-weight transmission. The DLR LWRIII [9] is a redundant robot with seven degrees of freedom, with a weight of 13.5 kg, and a load to weight ratio of 1:1. It has joint torque sensors in each joint and redundant position measurement (on motor and link side). In addition to the position and velocity interface, it has a torque control interface, enabling high performance soft robotics control.

### 1.1.3 Complaint Actuators

A more popular approach to create intrinsically safe robots is to make them compliant [10,11]. Even if collision avoidance can be implemented by sensors and artificial intelligence, it is still preferable to design robots that are physically unable to hurt people during unexpected collisions [12].

Series Elastic Actuator (SEA) [10] places an elastic component between the actuator and the robot link. SEA turns the force control into a position control problem, greatly improving force accuracy. The force control is achieved by controlling the position of the elastic element. This approach can lower the total impedance of a set of motor and gearbox. SEA can offer many benefits when compared to traditional stiff actuators. These benefits include shock tolerance, lower reflected inertia, more accurate and stable force control, and less damage to the environment. However, a drawback of this design is the control of the applied force using an elastic element. The use of an elastic element limits the control bandwidth of the actuation system as such SEA suffers from limited-bandwidth.

Variable Stiffness Actuator (VSA) [11] was introduced later to address the shortcoming of SEA. VSA has ability to alter the stiffness of the transmission coupling such that it becomes more compliant during high velocity tasks and stiffer during low velocity tasks. However, limited-bandwidth of the SEA approach still leads to limited dynamic performance in VSAs. Variable Impedance Actuators (VIAs) [13, 14] was also introduced upon the concept of VSA. VIA was realized based on varying the mechanical impedance (i.e. stiffness, damping, and/or gear-ratio parameters) of the actuation subsystem. VIA was designed to achieve fast motion control while guaranteeing safety of the actuation system.

Distributed macro-mini actuation ( $DM^2$ ) [15] was introduced to maintain the inherent safety, while preserving performance.  $DM^2$  actuation approach utilizes a parallel combination of low and high frequency actuators. In this concept low-frequency high-torque actuators are used to do the heavy-lifting jobs, while the high-frequency torque actuation is maintained using small motors. For the high-frequency actuation, very low impedance is achieved by connecting the motor to the manipulator through low-friction, low-reduction cable transmissions. As for low frequencies, low impedance is achieved using series elastic actuators (SEA). This concept has been employed in the actuation mechanisms of a 2-DOF arm [16] and a 3-DOF “Human-Friendly Robot” (HFR) [17].



### 1.1.4 Variable Damper Actuators

An alternative to Series Elastic Actuator (SEA) is the Series Damper Actuator (SDA) which incorporates a series damper instead of a series elastic component between the actuators and the load [18]. This configuration allows controlling the output torque of the actuator based on the relative angular velocity between the motor and the damper. SDA was then extended to Variable Damping Actuation (VDA) [19]. Variable dampers are realized depending on their different operating principles [20]; friction dampers, Electro-Rheological and Magneto-Rheological dampers, Eddy current dampers, fluid dynamics dampers.

### 1.1.5 Distributed Active Semi-Active Actuation Approach

Distributed Active Semi-Active Actuation (DASA) [21] is our approach for delivering safe and performant actuation. DASA approach breaks down the actuation into two elements; an active element such as an electric motor and a semi-active element that is a Magneto-Rheological (MR) clutch. The active element is responsible for generating the actuation power while the semi-active element is responsible for delivering the actuation power to the load. This approach allows multiple semi-active elements (i.e. MR clutches) at different locations to be driven using a single active element (e.g. motor). In a robot, the semi-active elements can be located at the joints and be all driven using a single active drive at the base of the robot [22, 23]. To enable independent motion of each joint two antagonistically driven semi-active elements are used at each joint. In this approach, known as Antagonistic-DASA (A-DASA) the motor provides input in opposite directions, clockwise and counter-clockwise, which enables a pair of antagonistically driven semi-active elements to drive each joint in either direction and independent from the other joints.

The building block of DASA and A-DASA is an MR clutch in which MR fluid is used as a means of torque transmission between the input and output of the MR clutch. The ability to change the viscosity of MR fluids rapidly and precisely give MR clutches desirable characteristics. MR clutches (subsequently DASA and A-DASA) can achieve high bandwidth in force/torque control [21, 24]. These devices can be built with high torque-to-mass and torque-to-inertia ratios and be utilized in medium to high torque demand robotic applications. MR clutches are full back-drivable devices and neither expensive nor technically complex.

## 1.2 Magneto-Rheological Devices and Actuators

Magnetorheological (MR) fluids are a class of smart materials composed of a carrier fluid, typically a type of oil or water, with suspended micron-sized particles. The viscosity of the fluid can be controlled by an external magnetic field through the alignment of the particles in the direction of the field in form of columns. The yield stress of the fluid is dependant on, and can be controlled with the intensity of the magnetic field. MR fluids follow the Bingham models: after a yielding point, they behave as viscous liquids. The Bingham visco-plastic model is commonly used to represent the shear stress of the fluid as a function of the applied field, and shear rate. Additional models have also been used to describe the non-linear behavior of MR fluids, such as Herschel-Bulkley model [25], and Bouc-Wen model [26]. MR fluids exhibit little or no hysteric behavior [27] and respond on the order of milliseconds [28].

Although being discovered in late 1940, MR fluids have only become commercially available recently. MR based devices have been widely used in many applications, such as damper in automotive industry [29], earthquake-proof structure [30–32], fan clutch [33].

Devices utilizing MR fluids have also been recognized in robotics, however almost entirely for use in haptic systems. Suitability of MR actuators in haptic interfaces is presented in [34]. Design and development of haptic devices based on MR fluids were presented in [35, 36]. Leg exoskeletons were implemented using promising electromagnetic structures of MR based actuators [37, 38]. Perpendicularly positioned MR actuators in a gimbal structure demonstrated the applications of the MR actuators in virtual reality [39]. More recently, the ability of MR actuators to enhance the safety of human-friendly robots based on the intrinsic passivity of MR actuators was discussed in [21, 40]. A normally closed (NC) type MR clutch using electromagnetic coil and a set of rare-earth permanent magnets as a safety device for human-collaborative robots is proposed in [41].

### 1.2.1 MR Fluid Durability

The study of MR fluids has become aligned with development of MR devices. Researchers are exploring new ways to develop more efficient MR fluids. MR fluids have shown some limitations that prevents their ability in different applications. Failures and defects such as hard cake, clumping effects, fluid particles separation (FPS) and particles oxidation require special attention to minimize the failure on MR fluids [42].

### **Hard cake**

Most MR fluids face problems due to sedimentation and the formation of hard cake in the absence of particular additives. The formation of hard cake is extremely hard to scatter due to existence of remnant magnetization between the particles. Proper choice of additives can insure that the MR fluid is stable against particle settling in different applications. In this regard, silicone oil based fluids have shown advantages in terms of deterioration especially if exposed to high temperatures for extended periods or to ionizing radiation [43].

### **Clumping effects**

Clumping effect occurs when MR fluids are exposed to higher magnetic field for a longer period of time. The iron particles in an MR fluid become entrapped in the chains that were formed under magnetic field. Clumping effect eventually makes the MR fluid stiffer

### **Particles oxidation**

MR fluids are mainly consist of 20-40% magnetic particle of various type such as carbonyl iron, stainless steel flakes, hydrogen reduced iron, and magnetic iron oxides. Iron based MR fluids suffer from oxidization if exposure to the atmosphere. Oxidation of particle alters the performance of an MR fluid due to chemical changes of the iron and demolishes magneto-rheological effect of the fluid.

A durability test of magneto-rheological fan clutch was conducted for 540 and 108 hours of service. Production of porous layer of magnetite on the particles surface proved that the iron particles oxides over time [44]. Another experiment of an automotive MR damper showed that the yield stress increases up to five times in the fluid off-state due to *in-use-thickening* (IUT) under the exposure to a long term loading simultaneously [45].

## **1.2.2 MR Fluid Characteristic**

The field dependent yield stress  $\tau$  and magnetic flux density  $B$  are expressed in terms of the magnetic field intensity  $H$  applied to the MR fluid, and are shown in Fig. 1.1 and Fig. 1.2, respectively. The field dependent yield stress and magnetic flux density versus magnetic field

intensity are a series of predicted curves based on “Dr. Dave” empirical equations [46]:

$$B = 1.91\phi^{1.133}(1 - e^{-10.97\mu_0 H}) + \mu_0 H \quad (1.1a)$$

$$\tau_y = 2.717 \times 10^5 C \phi^{1.5239} \tanh(6.33 \times 10^{-6} H) \quad (1.1b)$$

where  $\phi$  is the volume fraction of iron particles,  $\mu_0 = 4\pi \times 10^{-7}$  is the permeability of the free space,  $\tau_y$  is the yield stress,  $H$  is the magnetic intensity, and  $C$  equals 1.0, 1.16 or 0.95 depending on whether the carrier fluid is hydrocarbon oil, water or silicone oil.

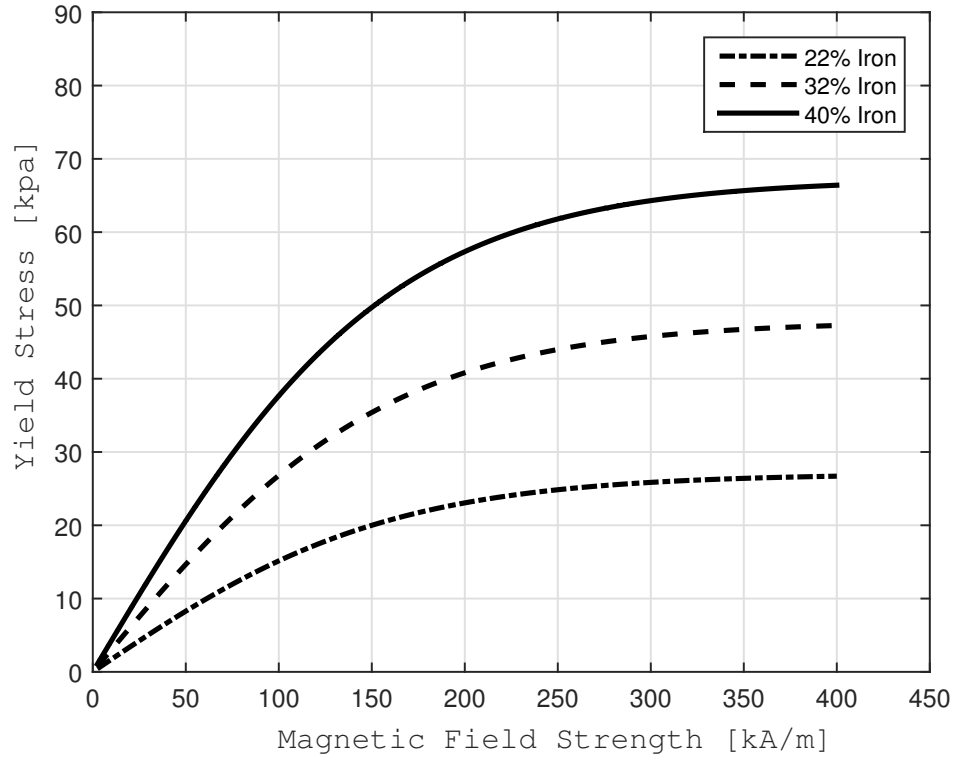


Figure 1.1: Yield Strength versus magnetic field strength of several typical MR fluids.

## 1.3 Objectives

The purpose of this work is to develop, optimize, and implement a new magnetic actuation mechanism in MR fluid based actuators used in robotic applications. The main objective of this work can be summarized as follow:

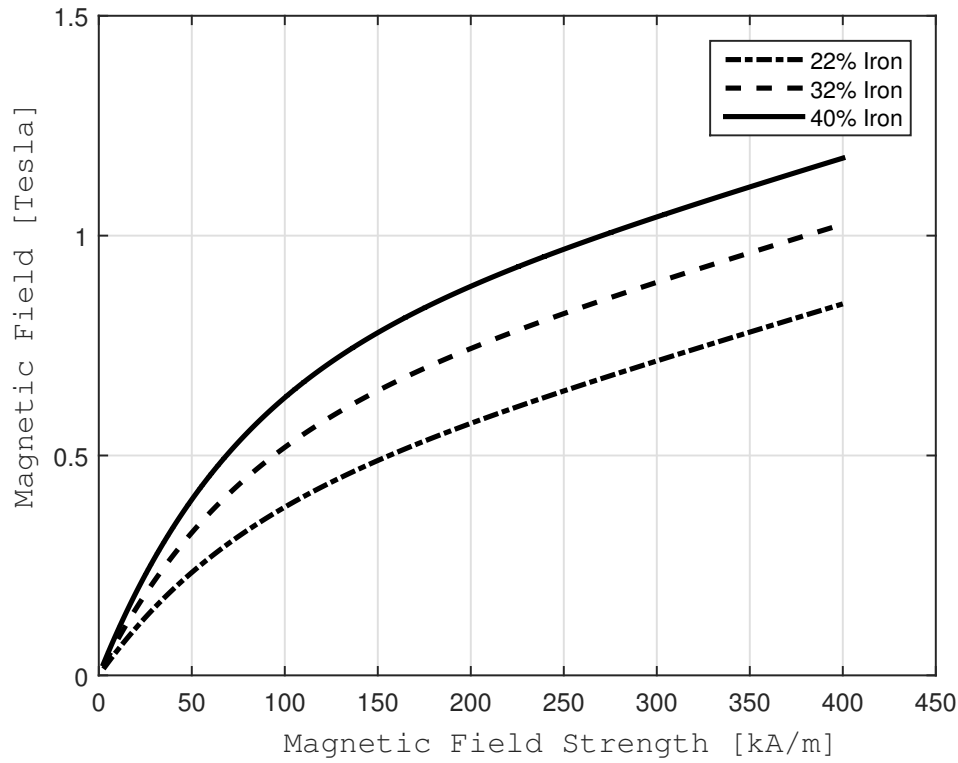


Figure 1.2: Magnetic field versus magnetic field strength of several typical MR fluids.

- The proposal of a new hybrid Magneto-rheological (MR) actuator using a parallel combination of electromagnetic coil and permanent magnet.
- Studying the performances of the optimized hybrid MR actuator with its coil-based counterpart.
- The design, and manufacturing of the proposed hybrid MR actuator.
- Modeling and control of the actuation mechanism.

### 1.3.1 Contributions

The major contributions of this dissertation are as follows:

#### **Introduction of a Hybrid MR Actuator**

In this work, a new concept for generating magnetic field in Magneto-Rheological (MR) clutches is presented. This concept breaks down the magnetic field generation into two parts using an electromagnetic coil and a permanent magnet. The combination of permanent magnets and electromagnetic coils in MR clutches allows to distribute the magnetic field inside an MR clutch more uniformly by relocating the areas in the magnetic path that are more prone to magnetic saturation. The permanent magnet also provides the clutch with an initial magnetic flux to keep the MR clutch at its optimal working point. The electromagnetic coil on the other hand adjusts the magnetic field to a desired value on demand.

#### **Development of a Hybrid MR Actuator**

A novel Hybrid MR Actuator (HMR) actuator using a parallel combination of electromagnetic coil and permanent magnet is developed and fabricated. The prototype HMR clutch is the newest generation of MR clutches introduced in our previous works. HMR clutch results in much favorable torque-to-mass ratio in comparison to its coil-based counterpart making them suitable for human safe robotic applications.

#### **Modeling Hysteresis in MR Actuators**

MR clutches suffer from the existence of nonlinear hysteretic behavior between their input and output. This behavior needs to be fully investigated in order to perform high fidelity force/torque control. An Artificial Neural Network (ANN) that uses magnetic field measurements from an embedded Hall sensor inside the clutch is trained to estimate the hysteretic behavior of the HMR clutch, and deal with unknown dynamics of the system. The developed neural network is capable of accurately predicting the transmitted torque as well as modeling the hysteretic relationship between the applied current, internal magnetic field within the clutch, and the output torque of the actuator. The effectiveness of the proposed method is experimentally validated.

### 1.3.2 Thesis Outline

The rest of this thesis is organized as follows, while the overlap between chapters are inevitable due to the integrated nature of the thesis.

In Chapter 2, the hybrid MR actuator using a parallel combination of permanent magnet and electromagnetic coil is introduced. Here, Finite Element Method (FEM) is hired to study the the intensity of the (quasi-static) magnetic field inside the clutch. FEM model of a previously built conventional MR clutch is experimentally validated to further investigate the preliminary behavior of the HMR clutch. An optimization problem is defined to compare the optimal designs of conventional and hybrid MR clutches.

In Chapter 3, the design procedure of the novel HMR clutch, as well as experimental validation are presented. Details regarding optimization, mechanical design, and fabrication are discussed. The dynamic performance of this actuation mechanism is then experimentally analyzed.

In Chapter 4, the non-linearity within the HMR clutch is discussed. Artificial Neural Network (ANN) is proposed to address the hysteresis in magnetic model of the HMR clutch. Extensive experimental results are presented in this chapter to validate the proposed ANN model

Finally, remarking conclusion are given in Chapter 5. This chapter also addresses the future work.

# Bibliography

- [1] B. Siciliano and O. Khatib, *Springer handbook of robotics*. Springer Science & Business Media, 2008.
- [2] M. Kermani and A. Shafer, “Magneto-and electro-rheological based actuators for human friendly manipulators,” Sept. 30 2014. US Patent App. 14/502,389.
- [3] A. Shafer, “Magneto-rheological fluid based actuator for human friendly robotic manipulators,” Master’s thesis, University of Western Ontario, 2009.
- [4] H. Inaba, M. Kita, S. Sakakibara, and R. Nihei, “Industrial robot with a safeguard mechanism,” Sept. 27 1983. US Patent 4,406,576.
- [5] D. M. Ebert and D. D. Henrich, “Safe human-robot-cooperation: Image-based collision detection for industrial robots,” in *Intelligent Robots and Systems, 2002. IEEE/RSJ International Conference On*, vol. 2, pp. 1826–1831, IEEE, 2002.
- [6] A. Garcia, V. Feliu, and J. Somolinos, “Experimental testing of a gauge based collision detection mechanism for a new three-degree-of-freedom flexible robot,” *Journal of Robotic Systems*, vol. 20, no. 6, pp. 271–284, 2003.
- [7] A. De Luca, A. Albu-Schaffer, S. Haddadin, and G. Hirzinger, “Collision detection and safe reaction with the dlr-iii lightweight manipulator arm,” in *Intelligent Robots and Systems, 2006 IEEE/RSJ International Conference on*, pp. 1623–1630, IEEE, 2006.
- [8] K. Salisbury, W. Townsend, B. Ebrman, and D. DiPietro, “Preliminary design of a whole-arm manipulation system (wams),” in *Robotics and Automation, 1988. Proceedings., 1988 IEEE International Conference on*, pp. 254–260, IEEE, 1988.



- [9] G. Hirzinger, N. Sporer, A. Albu-Schaffer, M. Hahnle, R. Krenn, A. Pascucci, and M. Schedl, “Dlr’s torque-controlled light weight robot iii-are we reaching the technological limits now?,” in *Robotics and Automation, 2002. Proceedings. ICRA’02. IEEE International Conference on*, vol. 2, pp. 1710–1716, IEEE, 2002.
- [10] G. A. Pratt and M. M. Williamson, “Series elastic actuators,” in *Intelligent Robots and Systems 95.’Human Robot Interaction and Cooperative Robots’, Proceedings. 1995 IEEE/RSJ International Conference on*, vol. 1, pp. 399–406, IEEE, 1995.
- [11] G. Tonietti, R. Schiavi, and A. Bicchi, “Design and control of a variable stiffness actuator for safe and fast physical human/robot interaction,” in *Robotics and Automation, 2005. ICRA 2005. Proceedings of the 2005 IEEE International Conference on*, pp. 526–531, IEEE, 2005.
- [12] N. Lauzier and C. Gosselin, “Series clutch actuators for safe physical human-robot interaction,” in *Robotics and Automation (ICRA), 2011 IEEE International Conference on*, pp. 5401–5406, IEEE, 2011.
- [13] G. Tonietti, R. Schiavi, and A. Bicchi, “Optimal mechanical/control design for safe and fast robotics,” in *Experimental Robotics IX*, pp. 311–320, Springer, 2006.
- [14] A. Bicchi, G. Tonietti, and R. Schiavi, “Safe and fast actuators for machines interacting with humans,” in *Robotics and Automation, 2004. TExCRA’04. First IEEE Technical Exhibition Based Conference on*, pp. 17–18, IEEE, 2004.
- [15] M. Zinn, B. Roth, O. Khatib, and J. K. Salisbury, “A new actuation approach for human friendly robot design,” *The international journal of robotics research*, vol. 23, no. 4-5, pp. 379–398, 2004.
- [16] M. R. Zinn, *A new actuation approach for human-friendly robotic manipulation*. Stanford University, 2005.
- [17] P. S. Thaulad, *Human Friendly Robot: Control System Design and Experimental Validation*. PhD thesis, Stanford University, 2005.

- [18] C.-M. Chew, G.-S. Hong, and W. Zhou, "Series damper actuator: a novel force/torque control actuator," in *Humanoid Robots, 2004 4th IEEE/RAS International Conference on*, vol. 2, pp. 533–546, IEEE, 2004.
- [19] M. Laffranchi, N. G. Tsagarakis, and D. G. Caldwell, "A variable physical damping actuator (vpda) for compliant robotic joints," in *Robotics and Automation (ICRA), 2010 IEEE International Conference on*, pp. 1668–1674, IEEE, 2010.
- [20] M. Catalano, G. Grioli, M. Garabini, F. W. Belo, A. D. Basco, N. Tsagarakis, and A. Bicchi, "A variable damping module for variable impedance actuation," in *Robotics and Automation (ICRA), 2012 IEEE International Conference on*, pp. 2666–2672, IEEE, 2012.
- [21] A. S. Shafer and M. R. Kermani, "On the feasibility and suitability of mr fluid clutches in human-friendly manipulators," *Mechatronics, IEEE/ASME Transactions on*, vol. 16, no. 6, pp. 1073–1082, 2011.
- [22] A. S. Shafer and M. R. Kermani, "Development of high performance intrinsically safe 3-dof robot," in *Robotics and Automation (ICRA), 2014 IEEE International Conference on*, pp. 619–624, IEEE, 2014.
- [23] P. Yadmellat, A. S. Shafer, and M. R. Kermani, "Design and development of a single-motor, two-dof, safe manipulator," *Mechatronics, IEEE/ASME Transactions on*, vol. 19, no. 4, pp. 1384–1391, 2014.
- [24] N. Takesue, J. Furusho, and M. Sakaguchi, "Improvement of response properties of mr-fluid actuator by torque feedback control," in *Robotics and Automation, 2001. Proceedings 2001 ICRA. IEEE International Conference on*, vol. 4, pp. 3825–3830, IEEE, 2001.
- [25] X. Wang and F. Gordaninejad, "Flow analysis of field-controllable, electro-and magnetorheological fluids using herschel-bulkley model," *Journal of Intelligent Material Systems and Structures*, vol. 10, no. 8, pp. 601–608, 1999.
- [26] B. Spencer Jr, S. Dyke, M. Sain, and J. Carlson, "Phenomenological model for magnetorheological dampers," *Journal of engineering mechanics*, 1997.

- [27] M. R. Jolly, J. W. Bender, and J. D. Carlson, "Properties and applications of commercial magnetorheological fluids," *Journal of intelligent material systems and structures*, vol. 10, no. 1, pp. 5–13, 1999.
- [28] K. D. Weiss and J. D. Carlson, "A growing attraction to magnetic fluids," *Machine design*, vol. 66, no. 15, pp. 61–64, 1994.
- [29] J. D. Carlson, M. J. Chrzan, and F. O. James, "Magnetorheological fluid devices," Feb. 8 1994. US Patent 5,284,330.
- [30] H.-J. Jung, B. F. Spencer Jr, and I.-W. Lee, "Control of seismically excited cable-stayed bridge employing magnetorheological fluid dampers," *Journal of Structural Engineering*, vol. 129, no. 7, pp. 873–883, 2003.
- [31] P. M. Todd and G. Gigerenzer, "Environments that make us smart ecological rationality," *Current Directions in Psychological Science*, vol. 16, no. 3, pp. 167–171, 2007.
- [32] Y. Xu, W. Qu, and J. Ko, "Seismic response control of frame structures using magnetorheological/electrorheological dampers," *Earthquake engineering & structural dynamics*, vol. 29, no. 5, pp. 557–575, 2000.
- [33] S. Gopalswamy, S. M. Linzell, G. L. Jones, W. C. Kruckemeyer, and G. L. Johnston, "Magnetorheological fluid fan clutch," Apr. 27 1999. US Patent 5,896,965.
- [34] N. Najmaei, M. R. Kermani, and R. V. Patel, "Suitability of small-scale magnetorheological fluid-based clutches in haptic interfaces for improved performance," 2015.
- [35] A. Bicchi, M. Raugi, R. Rizzo, and N. Sgambelluri, "Analysis and design of an electromagnetic system for the characterization of magneto-rheological fluids for haptic interfaces," *Magnetics, IEEE Transactions on*, vol. 41, no. 5, pp. 1876–1879, 2005.
- [36] B. Liu, W. Li, P. B. Kosasih, and X. Zhang, "Development of an mr-brake-based haptic device," *Smart Materials and Structures*, vol. 15, no. 6, p. 1960, 2006.
- [37] O. Baser and M. A. Demiray, "Selection and implementation of optimal magnetorheological brake design for a variable impedance exoskeleton robot joint," *Proceedings of the Institution of Mechanical Engineers, Part C: Journal of Mechanical Engineering Science*, p. 0954406215627180, 2016.

- [38] J. Chen and W.-H. Liao, "Design and control of a magnetorheological actuator for leg exoskeleton," in *Robotics and Biomimetics, 2007. ROBIO 2007. IEEE International Conference on*, pp. 1388–1393, IEEE, 2007.
- [39] W. Li, B. Liu, P. B. Kosasih, and X. Zhang, "A 2-dof mr actuator joystick for virtual reality applications," *Sensors and Actuators A: Physical*, vol. 137, no. 2, pp. 308–320, 2007.
- [40] P. Fauteux, M. Lauria, B. Heintz, and F. Michaud, "Dual-differential rheological actuator for high-performance physical robotic interaction," *Robotics, IEEE Transactions on*, vol. 26, no. 4, pp. 607–618, 2010.
- [41] T. Saito and H. Ikeda, "Development of normally closed type of magnetorheological clutch and its application to safe torque control system of human-collaborative robot," *Journal of Intelligent Material Systems and Structures*, vol. 18, no. 12, pp. 1181–1185, 2007.
- [42] S. Wahid, I. Ismail, S. Aid, and M. Rahim, "Magneto-rheological defects and failures: A review," in *IOP Conference Series: Materials Science and Engineering*, vol. 114, p. 012101, IOP Publishing, 2016.
- [43] J. D. Carlson, "MR fluids and devices in the real world," *International Journal of Modern Physics B*, vol. 19, no. 07n09, pp. 1463–1470, 2005.
- [44] J. C. Ulicny, M. P. Balogh, N. M. Potter, and R. A. Waldo, "Magnetorheological fluid durability testiron analysis," *Materials Science and Engineering: A*, vol. 443, no. 1, pp. 16–24, 2007.
- [45] J. Roupec and I. Mazurek, "Stability of magnetorheological effect during long term operation," in *Mechatronics*, pp. 561–567, Springer, 2011.
- [46] J. D. Carlson, "MR technology workshop- chapter 6," tech. rep., Lord Corporation, 2004.

## Chapter 2

# Design and Development of a Hybrid Magneto-Rheological Actuator

*The material presented in this chapter is published in the proceeding of "IEEE International Conference of Robotics and Automation (ICRA)," pp. 3083-3088, Stockholm, Sweden, 2016, doi:10.1109/ICRA.2016.7487474.*

In this chapter, we present a new concept for generating magnetic field in Magneto-Rheological (MR) clutches intended for safe robotic applications. The main rationale behind this concept is to divide the magnetic field generation into two parts using an electromagnetic coil and a permanent magnet. The permanent magnet generates a bias magnetic field density at the optimum working point of the MR clutch while the energized coil can add or negate the magnetic field to a desired value. The results will show clear advantages of this concept in reducing the total weight of the MR clutch, improving the torque-to-mass ratio, and reducing electrical power consumption. The proposed concept is validated using computer model of an MR clutch and Finite Element Method (FEM) is hired to compare the characteristics of the proposed MR clutch with those from conventional coil based clutch. Experimental results will be provided to further validate the advantages of the proposed new concept.

## 2.1 Introduction

In the late 1940, Magneto-Rheological (MR) fluids were discovered with the capability of changing their shear strength within few milliseconds [1] in response to external magnetic fields. This capability of MR fluids made them a good candidate for the development of automatic clutch devices. However, MR fluids have only become commercially available recently and being widely used in automotive and structural engineering in form of a damper. More recently, there has been more efforts towards the development of MR fluid-based devices as variable resistance brakes and clutches.

In most MR clutches electromagnetic coils have been used as the primary source of actuation to control the output torque of the MR clutch. The use of permanent magnets (PMs) as the primary actuation source in MR clutches has received less attention though. A fail-safe MR device excited by permanent magnets was proposed in [2]. The device was designed to engage and disengage a power brake vacuum pump from a diesel engine. A two-way MR fluid valve using a permanent magnet and a coil was discussed in [3]. The drawback of this design was the location of the permanent magnet that required the rated current of the coil to be carefully chosen in order not to outdo the coercivity of the PM. A normally closed (NC) type clutch using MRFs and rare-earth permanent magnets as a safety device for human-collaborative robots was studied in [4]. Under normal circumstances, the maximum torque would be transmitted through the clutch. The maximum torque was dictated by the power of the permanent magnet, while energizing the coil negates the magnetic bias of the PM. To the best of our knowledge, the use of PM and magnetic coil as proposed here has never been reported in the literature.

The main contributions of this work is the introduction of a new concept to combine a PM and an electromagnetic coil for magnetic field generation. This new concept results in significant reduction in the weight and electric power consumption in MR clutches. A new scheme to design, develop, and implement a hybrid MR clutch is also presented. Comparison results between hybrid MR clutches that use permanent magnets and electromagnetic coils and conventional coil based MR clutches are presented to validate our claims.

Compliant actuators are meant to disengage the reflected inertia of the actuator from the output link by integrating an elastic [5] or a damper [6] element into the transmission mechanism. The use of a compliant interface reduces impact forces and adds to the safety of the actuation paradigm. In this regard, MR clutches have been found to be advantageous to replace

the reflected inertia of the motor and gearbox with the inertia of the MR clutch itself [7]. This property of MR clutches lends itself to an excellent actuation alternative for safe human-robot collaborations. The higher torque-to-mass and torque-to-inertia ratios of the MR based actuators improve intrinsic safety characteristics of the actuation dramatically. In this paper it is shown that hybrid MR clutches can offer much favorable torque-to-mass ratio than their coil based counterparts. The combination of permanent magnets and electromagnetic coils in MR clutches allows to distribute the magnetic field inside an MR clutch more uniformly by relocating the areas in the magnetic path (such as the main shaft) that are more prone to magnetic saturation. By avoiding saturation, one can reduce the volume of material used in the magnetic path, *ergo* reducing the total mass of actuator and improving its inherent safety characteristics even further.

The organization of this chapter is as follow: Section 2.2 introduces MR clutches and derives the relationship between electrical and mechanical inputs and the output torque. Section 2.3 presents computer model verification of our previously manufactured MR clutch using experimental results. Section 2.4 introduces the permanent magnet based MR clutch, compares conventional and hybrid MR clutches, and presents a new hybrid MR clutch with optimal design. The last section concludes how the use of permanent magnets and electromagnetic coils can improve the functionality and characteristic of an MR clutch in terms of weight, compactness, and the output torque.

## 2.2 MR Actuator

Magnetorheological (MR) fluids are a class of smart materials composed of a carrier fluid, typically a type of oil or water, with suspended micron-sized particles. The viscosity of the fluid can be controlled with an external magnetic field through the alignment of the particles in the direction of the field in form of columns. The yield stress of the fluid is dependant on the intensity of the magnetic field. The efficiency of the fluid is judged using its yield stress,  $\tau_y$  that measures the strength of the column structure formed by the electromagnetic coil. The rotation of the input shaft of an MR clutch under the influence of an induced field, causes shearing in MR fluid resulting in the rotation of the output shaft.

Fig. 2.1 depicts the cross section of a typical multi-disk MR clutch. It consists of stacks of input and output disks arranged around the rotational axis of the clutch with the space between

them filled with MR fluids. A yoke is required to close the magnetic circuit. An MR clutch is being controlled using both electrical and mechanical inputs, the latter is often kept constant. Thus the output of the system is controllable mainly using the electrical input. When the electromagnetic source is energized, the shear stress of the MR fluid is altered (increased) within the magnetic path, allowing the MR clutch to transmit the input mechanical power to its outer part.

The changes in the viscosity of MR fluids in response to an applied magnetic field follow the behavior of a Bingham fluid with high viscosity and low liquidity. Additional models have been used to describe the non-linear behavior of MR fluids, such as Herschel-Bulkley model [8], and Bouc-Wen model [9]. However, these models are complex and do not offer significant advantages for most common applications of MR clutch such as the one described in this paper. We use a Bingham plastic model to describe the behavior of MR fluids in the multi-disk MR devices as follows [10],

$$\tau = \tau_y(B) + \eta \frac{dv}{dz}, \tau > \tau_y \quad (2.1)$$

where  $\tau$  is the shear stress,  $\tau_y$  is the field dependent yield stress,  $B$  is the magnetic field,  $\eta$  is the Newtonian viscosity, and  $\frac{dv}{dz}$  is the velocity gradient in the direction of the field. The velocity gradient in (2.1) can be assumed constant. Under conditions discussed in [7], the model can be presented as,

$$\tau = \tau_y(B) + \eta \frac{\omega r}{l_f}, \tau > \tau_y \quad (2.2)$$

where  $\omega$  is the relative angular velocity between input and output of the clutch,  $l_f$  is the thickness of MR fluid gap between input and output disks, and  $r$  is the radius from the rotational axis. In a multi-disk MR clutch (e.g., Fig. 2.1), the transmitted torque is given by,

$$dT = 2\pi r^2 \tau dr. \quad (2.3)$$

where  $r$  is the radius from the shaft, and  $\tau$  is given in (2.2). The torque produced by an  $N$ -disk MR actuator can be expressed by integrating (2.3) along both sides of each MR gap as follows,

$$T = 4N\pi \left( \frac{\tau_y(B)(R_2^3 - R_1^3)}{3} + \frac{\eta\omega(R_2^4 - R_1^4)}{4l_f} \right) \quad (2.4)$$

where  $R_1$  and  $R_2$  are the inner and outer radius of the disks, respectively. The field dependant yield stress used in (2.4) can be expressed in terms of the magnetic field intensity applied to



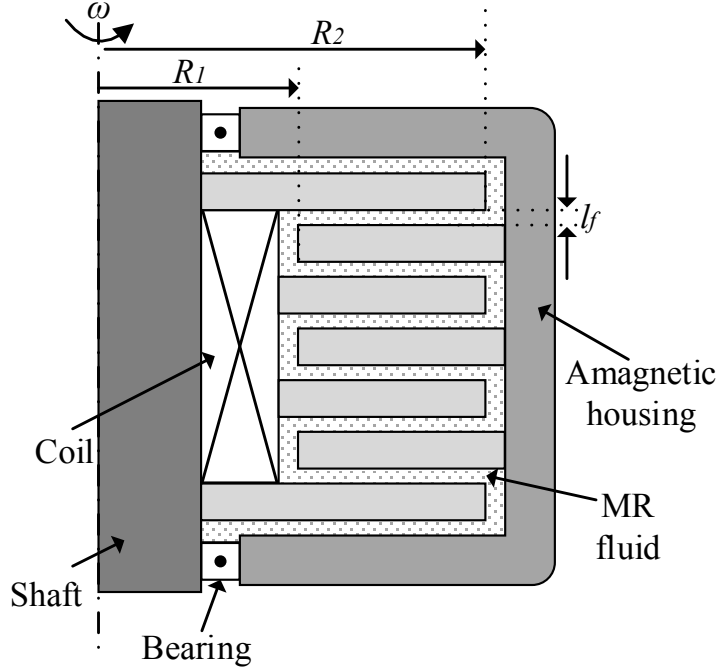


Figure 2.1: Cross-section of a multi-disk MR clutch.

the MR fluid and the material properties of the MR fluid, i.e.,

$$\tau_y = 2.717 \times 10^5 C \phi^{1.5239} \tanh(6.33 \times 10^{-6} H) \quad (2.5)$$

where  $\tau_y$  is the yield stress in Pa,  $\phi$  is the volume fraction of iron,  $H$  is the magnetic intensity, and  $C$  depends on the carrier fluid; for hydrocarbon oil  $C = 1$ .

### 2.2.1 MR Clutch Modeling Using FEM

The characteristic of an MR clutch can be modelled using Finite Element Method (FEM). The hysteresis behavior of the ferromagnetic materials though cannot be easily integrated into the computer model. Nevertheless, the model still provides substantial information regarding the intensity of the (quasi-static) magnetic field inside the clutch, the relationship between the input current and the magnetic field, and the output torque of the clutch with respect to the magnetic field. COMSOL Multiphysics® is a suitable software platform for developing models based on FEM. Using (2.4) and (2.5) in our model, we can predict the transmitted torque as a function of magnetic field strength within each MR fluid gap. The second term in the right hand side of (2.4) can be ignored due to the small differences between the input and output angular velocities of the MR clutch and the small value of Newtonian viscosity [11].

The computationally expensive nature of this type of modeling prohibits its use in control applications. However, the model is sufficiently accurate to lead the design and optimization of a particular design concept.

## 2.3 MR Clutch Model Verification

In our previous work, we compared multiple configurations of MR clutches and the effect of each configuration on the weight and electrical power consumption of an MR clutch [12]. In these studies, FEM was used as the main tool to estimate the magnetic field inside an MR clutch and predict the characteristics of the clutch. It was shown that for high-torque density MR clutches, a multi-disk configuration exhibited the best characteristics considering compactness, weight, and moment of inertia. The results were further validated in practice using a prototype MR clutch such as the one shown in Fig. 2.2. The specifications of the MR clutch shown in this figure are listed in Table 2.1.

Table 2.1: MR clutch specifications

Outer diameter [mm]	149
Maximum width [mm]	62
Disk thickness [mm]	1
MR fluid gap thickness [mm]	0.2
No. of input disks	4
Maximum torque [Nm]	10
Total mass [kg]	2.2

The objective of the current study is to use similar FEM to direct the design of a hybrid MR clutch. To this effect, we will first present the comparison results between an FEM based model of the MR clutch shown in Fig. 2.2 and those obtained experimentally in order to demonstrate the efficacy of the modeling technique. Next we will use the same modeling technique to direct the design of the new hybrid MR clutch. The experimental test bench used to obtain the results for comparison includes a brushless DC motor (BLWRPG235D-36V-4000-RI3) to provide the rotational inputs to the MR clutch. The motor is driven by a driver in the velocity control mode. A high-power motor driver (AMC-AZ12A8), set in current mode, is used to control the

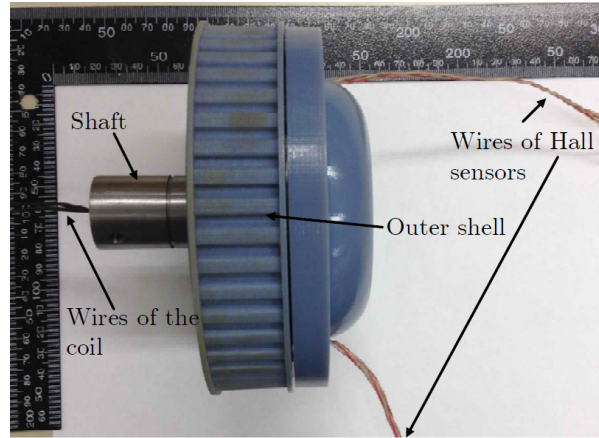


Figure 2.2: The optimal designed MR clutch.

current to the MR clutch. An ATI gamma F/T sensor is employed to read the output torque and A dSPACE (DS 1103) controller board to acquire data at a sampling frequency of 10 kHz. To measure the magnetic field intensity inside the MR clutch, two unipolar ratiometric Hall sensors (TLE4990 Infineon) are embedded inside the clutch.

In order to validate the FEM model, a low-frequency sinusoidal current varying between 0 and 1.3A (a dc offset is added to input current in order to provide positive current all the time to the actuator) was applied to the prototype MR clutch and the magnetic field intensity and the output torque were simultaneously measured. Fig. 2.3 depicts the input current, and the resulting magnetic flux density inside the clutch and its corresponding output torque.

The experimental results illustrate well agreement with those obtained from the model, verifying that the model developed in COMSOL Multiphysics® can estimate the characteristics of an actual MR clutch with sufficient accuracy. Fig. 2.4 also shows that the Bingham model is not capable of fully capturing hysteretic behavior of the MR clutch between its input current and output torque. Unlike control applications in which consideration of hysteresis can be quite important, in the current study the shortcoming of the FEM based model will not be detrimental to the results of the study.

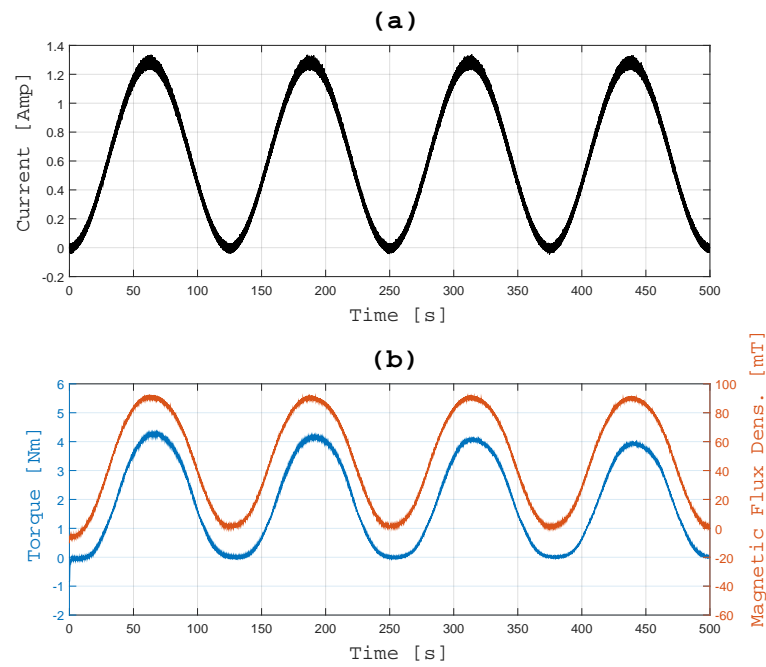


Figure 2.3: (a) Sinusoidal+DC component input current, (b) Output torque and magnetic flux density of the prototyped MR clutch.

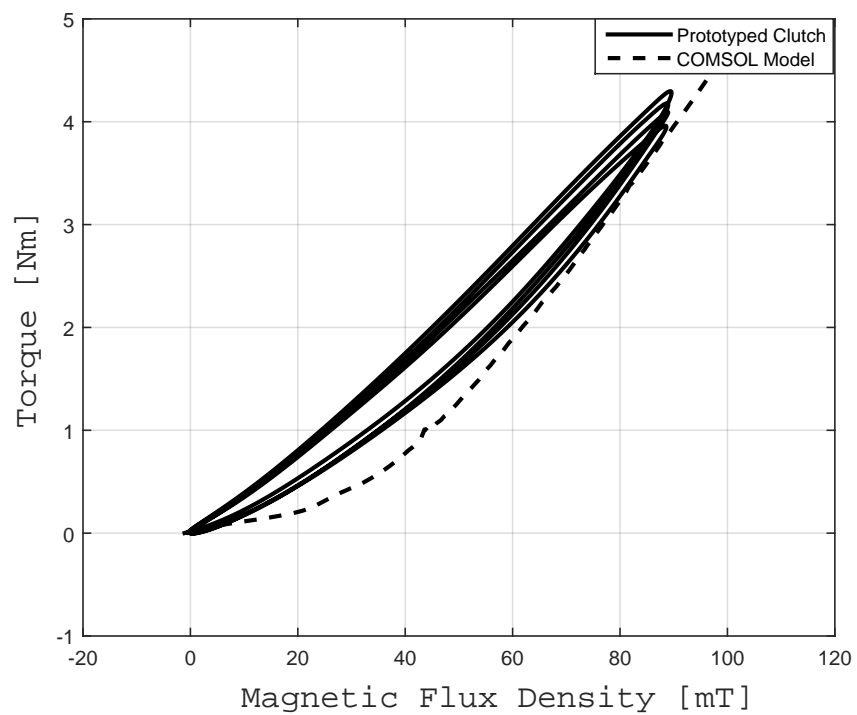


Figure 2.4: Comparison between measured results and simulation.

## 2.4 Permanent Magnet Based MR Clutch

In this section, the use of permanent magnets as part of magnetic field generation inside an MR clutch is discussed. The main idea behind employing a permanent magnet is to develop the magnetic field inside the MR clutch using a combination of an electromagnetic coil and a permanent magnet. The permanent magnet provides the clutch with an initial magnetic flux to keep the MR clutch at its optimal working point. The electromagnet coil on the other hand adjusts the magnetic field to a desired value on demand.

The permanent magnet (PM) used in our design is hollow cylindrical and located around the electromagnetic coil. The location of the permanent magnet is selected as part of the optimization process such that it results in best possible torque-to-mass ratio. The novelty of the proposed design is that it allows to achieve absolute zero and maximum torques using minimal magnetic flux (both low and high) levels in the MR fluid gaps.

Fig. 2.5 depicts the schematic of a hybrid MR clutch along with the magnetic field distributions inside the clutch. As shown in Fig. 2.5 A, the magnetic fields generated by the permanent magnet crosses the MR fluid, resulting in partial torque generation in the MR clutch. The strength of the PM is enough to keep the MR clutch at its optimal operating point. The optimal working point purely depends on the magnetic characteristics (B-H curve) of the MR clutch.

The electromagnetic coil makes up for the other part of the magnetic field as shown in Fig. 2.5 B and C. As observed, the magnetic flux of the electromagnetic coil depending on the polarity of the input current can be either added to or subtracted from that of the PM. This allows to generate the maximum torque and also to achieve absolute zero torque by generating sufficient opposite flux to cancel out the PM flux as well as hysteresis remanence. This configuration allows to relocate the areas of the magnetic circuit that are prone to saturation to other locations less likely to saturate. In this way, the current density of the coil *ergo* the MR clutch torque can be increased before the magnetic circuit becomes saturated or equivalently for a given value of the current density the mass of the MR clutch can be reduced by using less ferromagnetic materials in the magnetic circuit.

### 2.4.1 Material Selection

It is essential to specify the materials considered for each component of the MR clutches since the permeability and the saturation values are important for the validity of the simulation re-

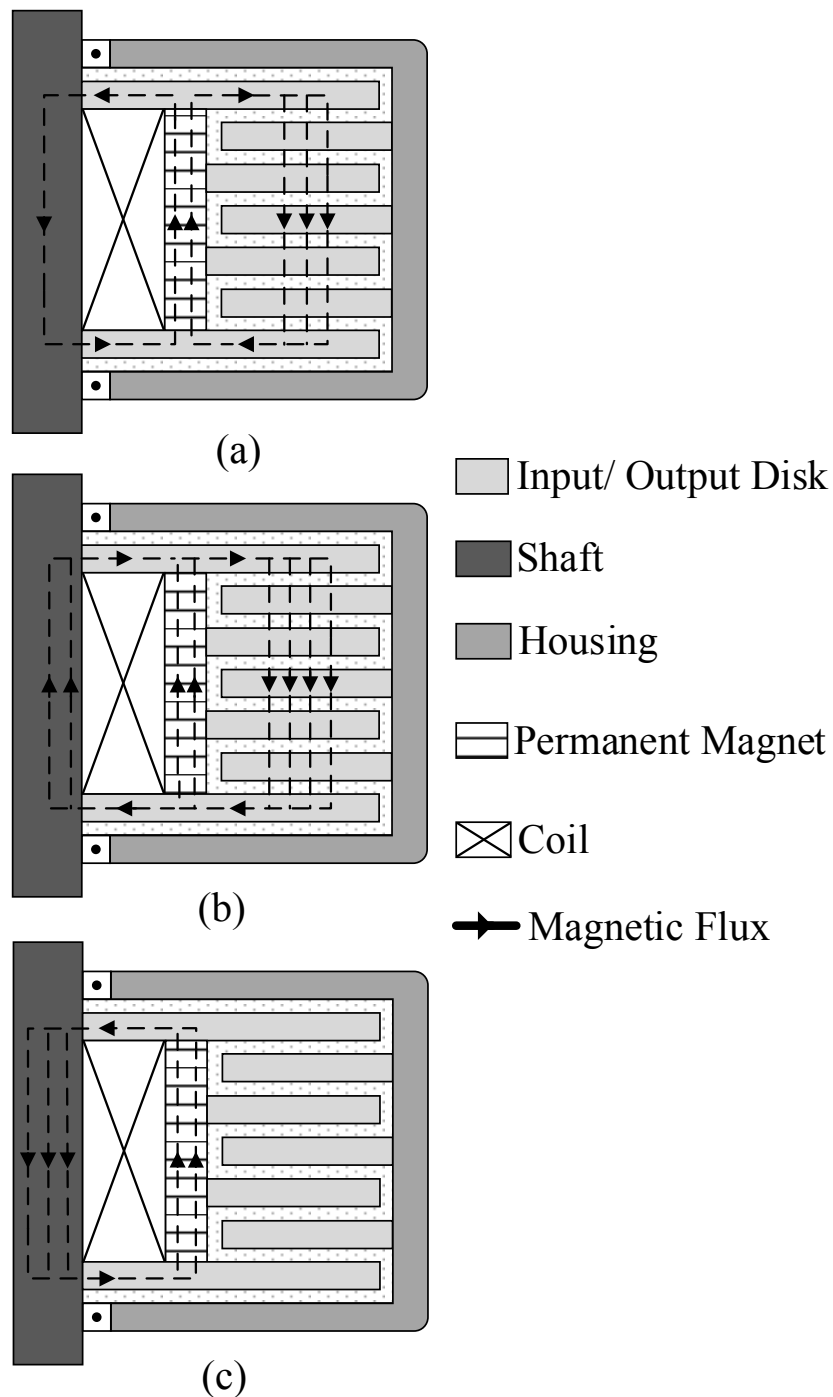


Figure 2.5: Magnetic field distribution inside a hybrid MR clutch: (a) magnetic flux density ( $B$  field) distribution inside the MR clutch due to the permanent magnet (off-state), (b) the field enhancement in the MR clutch pack with an applied magnetic field, and (c) the field cancellation in the MR clutch pack due to an applied magnetic field in reverse direction.

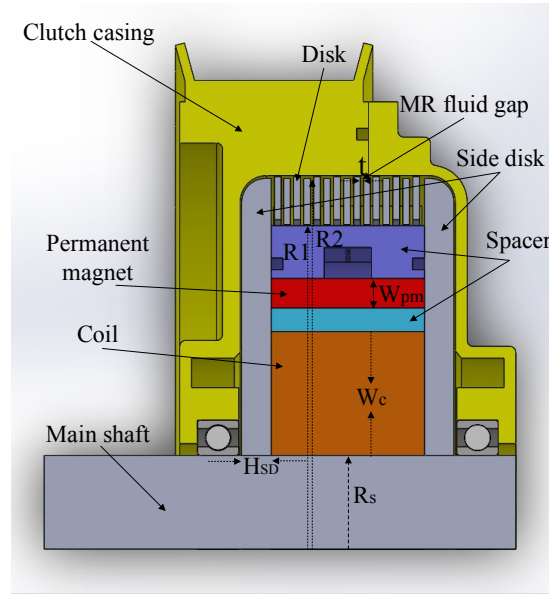


Figure 2.6: Parameters and functional components of a hybrid MR clutch.

sults. AISI steel 1018 was selected for the ferromagnetic component carrying the magnetic flux. The ferromagnetic components of the MR clutch are the shaft, input-output disks, and side disks. A non-magnetic material was used as the spacer between the disks and to separate the clutch pack from the clutch casing. Copper was selected for the coil. Neodymium N45 magnet was used as the permanent magnet based on the simulation results and availability. Lastly, MRF-140CG fluid was selected as the MR fluid inside the clutch.

## 2.4.2 Optimization

In this section the optimization of a hybrid MR clutch based on the FEM based model of the clutch is presented. The parameters considered for the optimization include the radius of the MR clutch's shaft, the inner and outer radii of the input and output disks, the thickness of the side disks, the geometry of electromagnetic coil and permanent magnet, coil's current density, and fluid gap thickness. Fig. 2.6 depicts these parameters. The objective of the optimization is to maximize the magnetic flux density within the MR fluid while minimizing the mass of the MR clutch for a given value of the nominal torque (e.g. in our case 15 Nm).

Full factorial design is investigated to achieve MR clutches configurations in response of every possible combination of design parameters. Different ranges of optimization vari-

Table 2.2: Optimization Variable

Variables	Corresponding Index	Range
Shaft radius [mm]	$R_s$	10-13
Disk width [mm]	$R_2 - R_1$	9-12
Side disk thickness [mm]	$H_{SD}$	3-6
Coil width [mm]	$W_c$	16-22
Permanent magnet Width [mm]	$W_{PM}$	2-5

ables are studied to obtain the convergence ranges. Shortened ranges are defined in COMSOL Multiphysics® to conduct the local search optimization. Table 2.2 lists the optimization variables and the range considered for each variable. The MR fluid gap is fixed to 0.4 mm and the thickness of the spacers separating the disks and the PM, and the electromagnetic coil and the PM are set to 5 mm and 3 mm, respectively.

The resulting torque-to-mass ratios for a hybrid MR clutch versus its nominal torque value for different number of the disks are shown in Fig. 2.7. Each point in this figure corresponds to a distinct combination of the optimization variables. As observed, the 6- and 8-disk configurations offer much higher torque-to-mass ratio for a given nominal torque value (e.g. 15 Nm). Also, the results indicate that the torque-to-mass ratio of a multi-disk hybrid MR clutch tends to increase for the higher values of the torque meaning that larger MR clutches are more efficient in packing more torque in a unit volume of the clutch.

To further investigate the results, the torque-to-mass ratio of a 6-disk hybrid MR clutch versus two critical design variables, i.e., the thickness of cap (side disk) and the radius of the shaft are shown in Fig. 2.8.

The results clearly illustrate the importance of the cap's (side disks' thicknesses. As observed increasing the thickness of the cap (side disk) from 3 mm to 5 mm results in twofold increase in the maximum torque of the MR clutch. The results also show that in the proposed configuration of the MR clutch, the diameter of the shaft does not affect the torque generation significantly. This indicates that unlike conventional MR clutches, the shaft in a hybrid MR clutch become less prone to magnetic saturation.

The following objective function was used to obtain the optimal design parameters of the



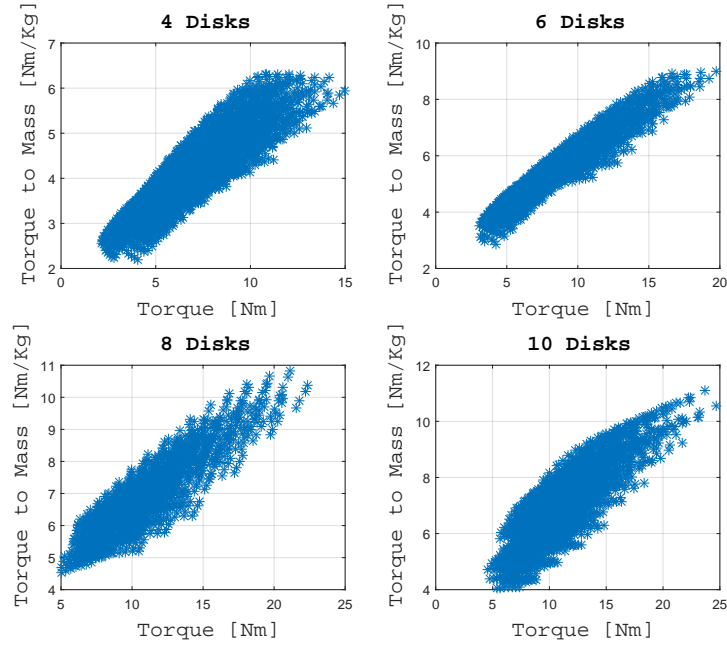


Figure 2.7: Torque-to-mass ratio vs. nominal torque.

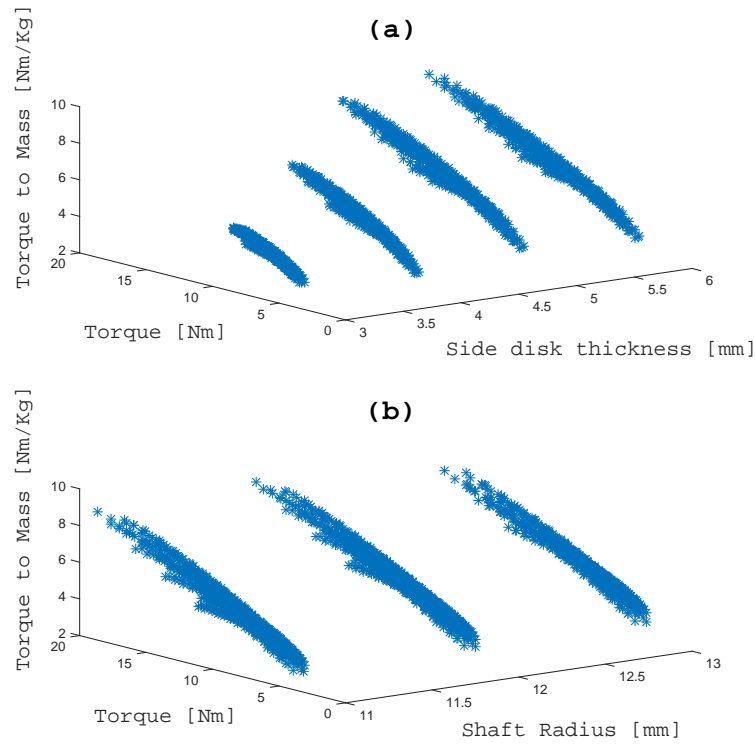


Figure 2.8: Torque-to-mass ratio of a 6-disk hybrid MR clutch vs (a) cap (side disk) thickness, and (b) shaft diameter.

6-disk hybrid as well as a conventional 6-disk MR clutch,

$$\begin{aligned} \min \quad & U = W_1|\tau_d - \tau_s| + W_2m_T + W_3\frac{1}{r_T} \\ \text{subject to} \quad & J_D \leq 2\frac{A}{mm^2} \end{aligned} \quad (2.6)$$

where  $W_1$ ,  $W_2$  and  $W_3$  are the weighting coefficients such that  $W_1 + W_2 + W_3 = 1$ ,  $\tau_d$  is the desired torque,  $\tau_s$  is the output torque of the clutch in the FEM based model,  $m_T$  is the mass,  $r_T$  is the torque-to-mass ratio and  $J_D$  is the current density applied to the coil.

### 2.4.3 Result Analysis

The optimization results are shown in Table 2.3. The reported output torques were calculated using (2.4) and (2.5). The estimated output torque for both configurations are almost 15 Nm. However, as observed, a hybrid MR clutch offers much better torque-to-mass ratio. Accordingly, the weight of an optimal hybrid MR clutch employing electromagnetic coil and PM can be reduced by 40 percent allowing to have a more compact and lightweight clutch. Furthermore, zero-current output torques were calculated for both configurations. In a hybrid MR clutch, the bias magnetic field generates a 3Nm bias torque. In a conventional MR clutch, the bias torque is negligible and not included in the FEM based model. Another important design consideration is the diameter of the shaft which is directly related to the moment of the inertia of the MR clutch. The hybrid MR clutch requires much smaller shaft in comparison to the conventional clutch for a given nominal torque value.

Figs. 2.9 and 2.10 illustrate the magnetic flux density contour in conventional and hybrid MR clutches when they are energized with the maximum current density. As seen the distribution of the saturation points is changed in the proposed hybrid MR clutch. Fig. 2.9 and 2.10 shows that in a conventional MR clutch, a saturation first happens at the intersection of the steel shaft and the side disks. The use of a PM however relocates the saturation point and helps the magnetic flux density to be distributed more uniformly within the magnetic circuit. Fig. 2.11 illustrates the formation of magnetic field within the clutch over time.

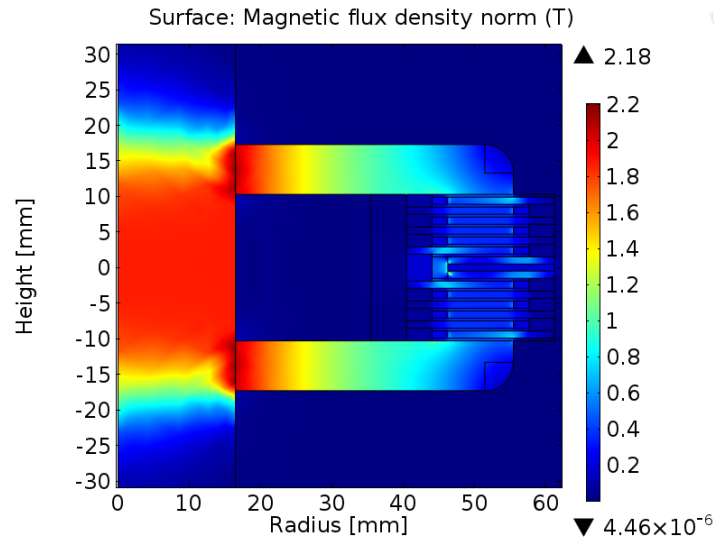


Figure 2.9: Magnetic flux density contour map in a conventional MR clutch.

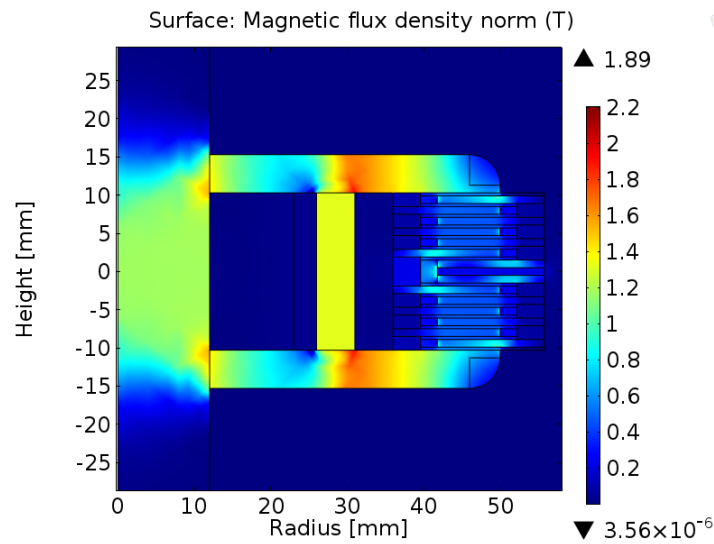


Figure 2.10: Magnetic flux density contour map in a Hybrid MR clutch.

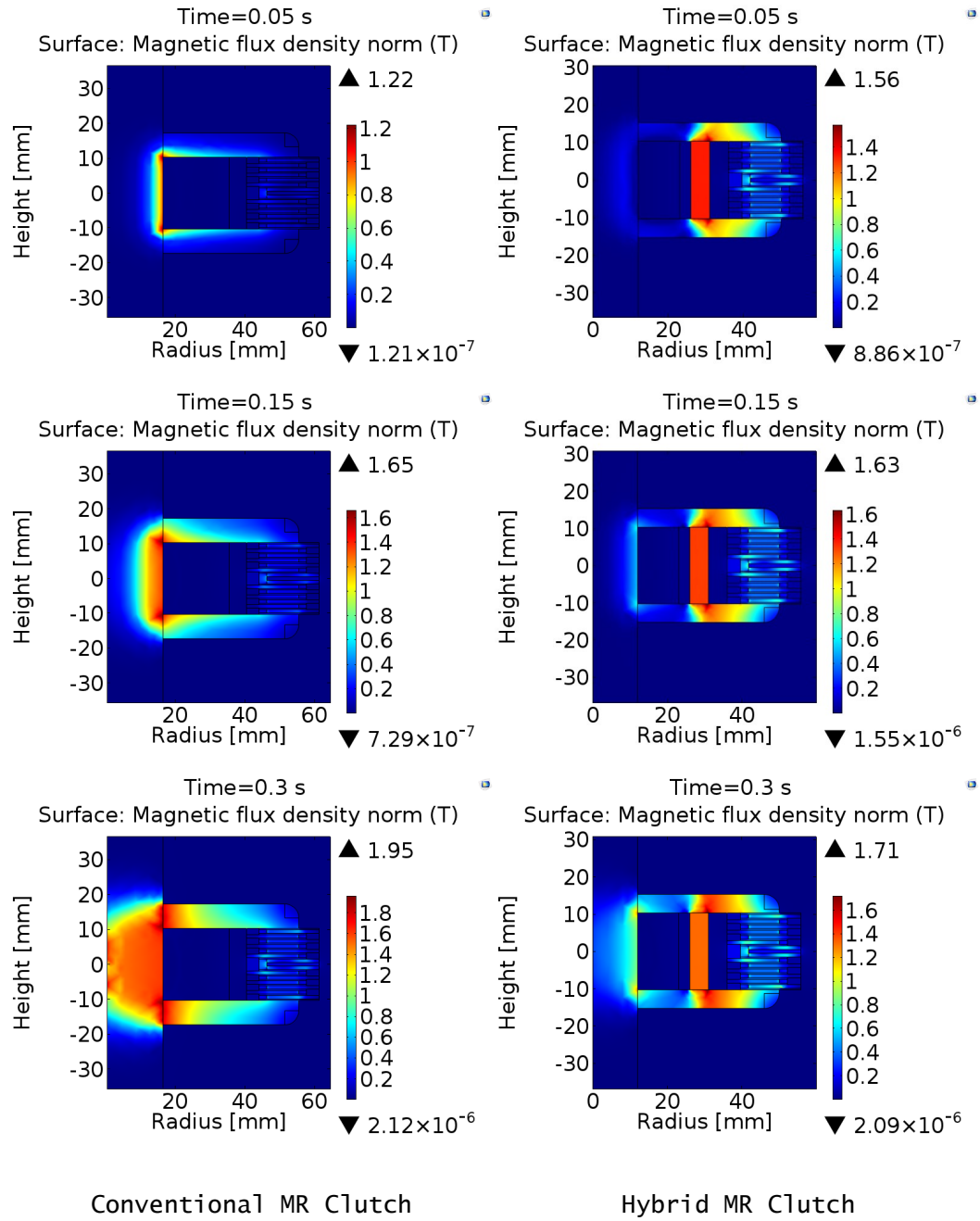


Figure 2.11: Preliminary results of the transient FEM analysis. Time evolution of the magnetic field at  $time = 0.05, 0.15, 0.30$  (s) is shown in both conventional and hybrid MR clutches.

Table 2.3: Comparison of conventional and hybrid MR clutches

	Conventional	Hybrid
Output Torque [Nm]	15.2	15.7
Mass [Kg]	2.73	1.6
Torque to Mass [ $\frac{\text{Kg}}{\text{Nm}}$ ]	5.56	9.81
Electrical Power Consumption [Watt]	6.7	2.6
Zero-current-applied torque [Nm]	0.03	3
Radius of Shaft [mm]	16.5	12
Total Diameter [mm]	123	111
Total Height [mm]	34.6	30.6

## 2.5 Conclusions

To further enhance the use of MR clutches in robotic applications, the idea of employing permanent magnet in MR clutches was introduced in this paper. Finite Element Method was used to design and optimize a hybrid MR clutch. The accuracy of the FEM based model was first verified using experimental data. Having verified the accuracy of the model, the model was then used to direct the design of the hybrid MR clutch. The results showed that using a PM in the construction of an MR clutch could significantly reduce the mass and inertia of the MR clutch for a given value of the nominal torque. In fact the results showed that using this technique the weight of an MR clutch could be reduced by as much as 40 percent. The light weight design of the MR clutches promotes the use of these devices in robotic applications requiring safe interactions with the humans.

# Bibliography

- [1] K. D. Weiss and J. D. Carlson, “A growing attraction to magnetic fluids,” *Machine design*, vol. 66, no. 15, pp. 61–64, 1994.
- [2] F. Bucchini, P. Forte, F. Frendo, A. Musolino, and R. Rizzo, “A fail-safe magnetorheological clutch excited by permanent magnets for the disengagement of automotive auxiliaries,” *Journal of Intelligent Material Systems and Structures*, p. 1045389X13517313, 2014.
- [3] G. Aydar, X. Wang, and F. Gordaninejad, “A novel two-way-controllable magnetorheological fluid damper,” *Smart Materials and Structures*, vol. 19, no. 6, p. 065024, 2010.
- [4] T. Saito and H. Ikeda, “Development of normally closed type of magnetorheological clutch and its application to safe torque control system of human-collaborative robot,” *Journal of Intelligent Material Systems and Structures*, vol. 18, no. 12, pp. 1181–1185, 2007.
- [5] G. Pratt, M. M. Williamson, *et al.*, “Series elastic actuators,” in *Intelligent Robots and Systems 95. Human Robot Interaction and Cooperative Robots*, *Proceedings. 1995 IEEE/RSJ International Conference on*, vol. 1, pp. 399–406, IEEE, 1995.
- [6] C.-M. Chew, G.-S. Hong, and W. Zhou, “Series damper actuator: a novel force/torque control actuator,” in *Humanoid Robots, 2004 4th IEEE/RAS International Conference on*, vol. 2, pp. 533–546, IEEE, 2004.
- [7] A. S. Shafer and M. R. Kermani, “On the feasibility and suitability of mr fluid clutches in human-friendly manipulators,” *Mechatronics, IEEE/ASME Transactions on*, vol. 16, no. 6, pp. 1073–1082, 2011.

- [8] X. Wang and F. Gordaninejad, "Flow analysis of field-controllable, electro-and magneto-rheological fluids using herschel-bulkley model," *Journal of Intelligent Material Systems and Structures*, vol. 10, no. 8, pp. 601–608, 1999.
- [9] B. Spencer Jr, S. Dyke, M. Sain, and J. Carlson, "Phenomenological model for magnetorheological dampers," *Journal of engineering mechanics*, 1997.
- [10] R. W. Phillips, *Engineering applications of fluids with a variable yield stress*. PhD thesis, University of California, Berkeley, 1969.
- [11] W. Li, P. Yadmellat, and M. R. Kermani, "Design optimization and comparison of magneto-rheological actuators," in *Robotics and Automation (ICRA), 2014 IEEE International Conference on*, pp. 5050–5055, IEEE, 2014.
- [12] W. Li, "Design and development of magneto-rheological actuators with application in mobile robotics.," Master's thesis, University of Western Ontario, London, Ontario, Canada, 2014.

## **Chapter 3**

# **Prototype Hybrid Magneto-Rheological Actuator**

In previous Chapter, the benefits of using permanent magnets (PM) in Magneto-Rheological (MR) fluid based actuators were studied. Our results showed that a combination of a permanent magnet and an electromagnetic coil resulted in much favorable torque-to-mass ratio in a Hybrid MR (HMR) clutch making these types of clutches more suitable for human safe robotic applications. This paper describes the design and development of a prototype HMR clutch and studies the dynamic performances of such a clutch for force/torque control, experimentally. The prototype HMR clutch used in the study is capable of transmitting up to 65Nm torque and has a control bandwidth of approximately 30Hz. The results show great potentials of this class of clutches for human-safe actuation systems.

### **3.1 Introduction**

In recent years, many developments in the field of the physical human robot interaction (pHRI) have been witnessed and significant attentions have been given to the subject of safety within the interactive environments. The result is a fundamentally different viewpoint towards the design of the robots and in particular their actuation systems. In conventional gear-base actuation system, a set of reduction gears are usually connected to an electric motor to increase the torque and decrease the speed. Since electric motors have poor torque density, considerable gear reduction is used to enable the required actuation. However, the addition of the gearing results



in an added reflected inertia and reflected damping in the output. The reflected inertia is often substantial since it is the inertia of the electric motor multiplied by the square of the gear ratio. In many occasions the reflected inertia is even larger than the inertia developed by the mass of the robot links [1]. Mismatch inertia between a motor and load can be minimized in order to optimize the dynamic performance and stability analysis [2]. However this optimization may not be cost effective or possible. Additionally, reduction gears introduce noise, backlash, and friction into the actuation system.

All of this has necessitated a need for new actuation approaches that lead to naturally low impedance. A compliant actuator is meant to achieve this by disengaging the reflected inertia of the actuator from the robot link. To this effect, Series Elastic Actuator (SEA) [3] places an elastic component between the motor and the robot link. This approach can lower the total impedance of a set of motor and gear box. However, a drawback of this design is the control of the applied force using an elastic element. The use of an elastic element limits the control bandwidth of the actuation system as such SEA suffers from limited bandwidth. Variable Stiffness Actuator (VSA) [4, 5] was introduced later to address the shortcoming of SEA. Another approach to safe actuation, while preserving performance was distributed macro-mini actuation ( $DM^2$ ) [1].  $DM^2$  actuation approach utilizes a parallel combination of low and high frequency actuators. Low-frequency high-torque actuators provide high torque components of a desired torque, while small motors provide high-frequency components of the desired torque.  $DM^2$  achieves low impedance using SEA located at the base of the robot and enhances the dynamic performance of the actuation by relying on small servo motors located at the joint.

Distributed Active Semi-Active Actuation (DASA) [6] is our approach for delivering safe and performant actuation. DASA approach breaks down the actuation into two elements; an active element such as an electric motor and a semi-active element that is a Magnet-Rheological (MR) clutch. The active element is responsible for generating the actuation power while the semi-active element is responsible for delivering the actuation power to the load. This approach allows multiple semi-active elements (i.e., MR clutches) at different locations to be driven using a single active element (e.g. motor). In a robot, the semi-active elements can be located at the joints and be all driven using a single active drive at the base of the robot [7, 8]. To enable independent motion of each joint two antagonistically driven semi-active elements are used at each joint. In this approach, known as A-DASA (A for Antagonistic) the motor provides input in opposite directions, clockwise and counterclockwise, which enables a pair of antagonisti-

cally driven semi-active elements to drive each joint in either direction and independent from the other joints.

The building block of DASA and A-DASA is an MR clutch in which MR fluid is used as a means of torque transmission between the input and output of the MR clutch. The ability to change the viscosity of MR fluids rapidly and precisely give MR clutches desirable characteristics. MR clutches (subsequently DASA and A-DASA) can achieve high bandwidth in force/torque control [9, 10]. These devices can be built with high torque-to-mass and torque-to-inertia ratios and be utilized in medium to high torque demand robotic applications. MR clutches are full back-drivable devices and neither expensive nor technically complex.

The contribution of this work is the introduction and validation of a new design concept for MR clutches that minimizes the power consumption and increase the torque density of the clutch. The idea is to use permanent magnets as a part of the magnetic field actuation along with an electromagnetic coil. It is shown that this concept can reduce the total weight of the clutch drastically in comparison to the conventional MR clutches. The combination of permanent magnets and electromagnetic coils in MR clutches allows to distribute the magnetic field carrying the magnetic flux inside the MR clutch more uniformly. The uniform distribution of the flux reduces the areas within the magnetic path that are prone to saturation. By avoiding saturation, one can reduce the volume of the material used in the magnetic path, therefore reducing the total mass of actuator. The inherent attributes of MR clutches such as high torque-to-mass and torque-to-inertia ratios, back-drivability, low inertia, and high bandwidth required for safe and performant actuation are preserved in Hybrid MR (HMR) clutches. This chapter discusses the design and development and presents experimental validations of a prototype HMR clutch with 65 Nm torque capacity. The suitability of the HMR clutch for physical human robot interaction (pHRI) applications are also discussed.

## **3.2 Design and Development of Hybrid MR Clutch**

### **3.2.1 Hybrid MR Clutch**

Magneto-rheological (MR) fluids are a class of smart materials composed of a carrier fluid, typically a type of oil or water, with suspended micron-sized particle. The viscosity of the fluid can be controlled with an external magnetic field that aligns the particles in the direction of the

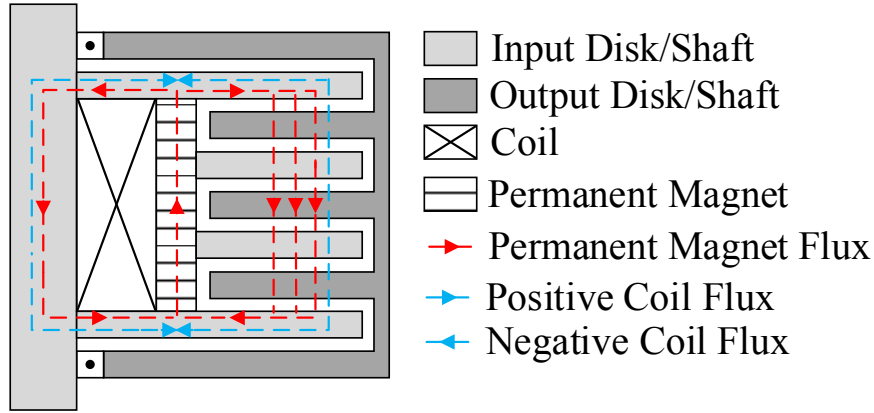


Figure 3.1: Cross-section of a hybrid MR clutch.

field. The yield stress of the fluid is dependent on the intensity of the magnetic field.

Fig. 3.1 shows the cross section of the proposed HMR clutch concept. As seen, a HMR clutch, not unlike a conventional MR clutch, consists of a stack of input and output disks arranged around the rotational axis of the clutch. The space between the disks is filled with MR fluids. The rotation of the input shaft in the presence of a magnetic field causes shearing in the MR fluid with respect to the output of the clutch, allowing the HMR clutch to transmit the input mechanical power to the outer part. The main difference between the two types of MR clutches is in the formation of the magnetic field using a combination of a coil and permanent magnet.

Regardless of the source of the magnetic field, it is the strength of the magnetic field that determines the amount of sheer stress developed inside the MR fluid as described by Bingham plastic model [11],

$$\tau = \tau_y(B) + \eta \frac{dv}{dz}, \quad \tau > \tau_y \quad (3.1)$$

where  $\tau$  is the shear stress,  $\tau_y$  is the field dependent yield stress,  $B$  is the magnetic field,  $\eta$  is the Newtonian viscosity, and  $\frac{dv}{dz}$  is the velocity gradient in the direction of the field. Due to the small values of viscosity  $\eta$ , the second term of (3.1) becomes negligible and is often ignored.

In a disk-type clutch, the torque generated across a circumferential element of a disk at a radius  $r$  is given by,

$$dT = 2\pi r^2 \tau dr. \quad (3.2)$$

The torque produced by an N-disk clutch is obtained after integrating (3.2) across the surface of  $N$  disks, yielding,

$$T = 4N\pi\left(\frac{\tau_y(B)(R_2^3 - R_1^3)}{3} + \frac{\eta\omega(R_2^4 - R_1^4)}{4l_f}\right) \quad (3.3)$$

where  $R_1$  and  $R_2$  are the inner and outer radius of the disks, respectively and all other parameters are as defined previously. The field dependent yield stress used in (3.3) can be expressed in terms of the magnetic field intensity applied to the MR fluid and the material properties of the MR fluid as in [12],

$$B = 1.91\phi^{1.133}(1 - e^{-10.97\mu_0 H}) + \mu_0 H \quad (3.4a)$$

$$\tau_y = 2.717 \times 10^5 C \phi^{1.5239} \tanh(6.33 \times 10^{-6} H) \quad (3.4b)$$

where  $\phi$  is the volume fraction of Iron,  $\mu_0 = 4\pi \times 10^{-7}$  is the magnetic constant,  $H$  is the magnetic intensity, and  $C$  is a constant that depends on the carrier fluid (e.g.,  $C = 1$  for hydrocarbon oil).

A HMR clutch takes advantage of a combination of electromagnetic coil and permanent magnet. By utilizing a permanent magnet, the clutch can partially transfer the input torque due to the induced magnetic field of the permanent magnet (shown using *red* flux lines in Fig. 3.1). When the electromagnetic coil is energized, the additional flux (shown using *blue* flux lines in Fig. 3.1) alters the (field dependant) shear stress of the MR fluid within the magnetic circuit, allowing to generate either minimum and maximum output torques depending on the polarity of the input current. To achieve absolute zero torque the input current must generate sufficiently opposing flux that cancels out the flux of the permanent magnet as well as the hysteresis remanence. The main benefit of this configuration is that it allows to relocate the areas of the magnetic circuit that are prone to saturation to other locations less likely to saturate. This ability allows us to reduce the volume of the magnetic material used to direct the magnetic field; thereby reducing the total weight of the HMR clutch. It was shown in our previous study [13] that the torque-to-mass ratio of an optimal HMR clutch can be as much as 40 percent higher than a conventional electromagnetic coil based MR clutch.

### 3.2.2 Design Of a Hybrid MR Clutch

A HMR clutch includes a number of input (output) magnetic disks spaced by nonmagnetic spacers to create a consistent gap between the disks for accommodating MR fluid and gener-

ating torque. Each disk has four angled fins and uses these fins to couple itself to the inner (outer) part of the clutch. Four dowel pins are used in each stack to interlock the input (output) disks together. Dowel pins help to distribute the torque uniformly across each stack and prevent backlash in the actuation. Two side plates are used to close the magnetic circuit path between the main shaft and the clutch pack. An exploded view of the magnetic disks and side plates is shown in Fig. 3.2(a).

The electromagnetic coil is wound on a magnetic bobbin which is keyed to the output shaft. Disks, side disks, and bobbin are made of high magnetically permeable materials to form a magnetic circuit within the clutch design. A hollow cylindrical shape permanent magnet is within the magnetic circuit to produce the bias electromagnetic flux. An insulation layer is placed between the clutch pack and the magnetic actuation components. The assembled HMR clutch is shown in Fig. 3.2(b). The casing of the clutch is designed such that it can receive the input torque generated by the active electric motor at the remote location through a transmission belt.

### 3.2.3 Actuator Mass

The mass of the HMR clutch can be obtained as

$$M = \rho_{st}(V_{sh} + V_{sd} + V_d) + \rho_{pm}V_{pm} + \rho_{MR}V_{MR} + \rho_{cu}V_{coil} \quad (3.5)$$

where  $\rho_{st}$ ,  $\rho_{pm}$ ,  $\rho_{MR}$ , and  $\rho_{cu}$  are the density of steel, permanent magnet, MR fluid, and copper respectively;  $V_{sh}$ ,  $V_{sl}$ ,  $V_{sd}$ ,  $V_d$ ,  $V_{pm}$ ,  $V_{MR}$ , and  $V_{coil}$  are the volume of the shaft, bobbin, side disk, disk, permanent magnet, MR fluid, and electromagnetic coil, respectively. However, mass of MR fluid is not considered in the simplified model due to its small volume value.

Fig. 3.3 shows the design parameters and the geometry of the HMR clutch. Describing the material volumes as a function of the design parameters gives total mass of the clutch as

$$V_{sh} = \pi R_{sh}^2 (H_c + 2H_{sd}) \quad (3.6)$$

$$V_{sl} = 2\pi H_c ((R_{sh} + w_{sl})^2 - R_{sh}^2) \quad (3.7)$$

$$V_{sd} = 2\pi H_{sd} (R_2^2 - R_{sh}^2) \quad (3.8)$$

$$V_{coil} = \pi (H_c) ((R_{sh} + w_{sl} + w_c)^2 - (R_{sh} + w_{sl})^2) \quad (3.9)$$

$$V_{pm} = \pi (H_c) ((R_{sh} + w_{sl} + w_c + w_{pm})^2 - (R_{sh} + w_{sl} + w_c)^2) \quad (3.10)$$

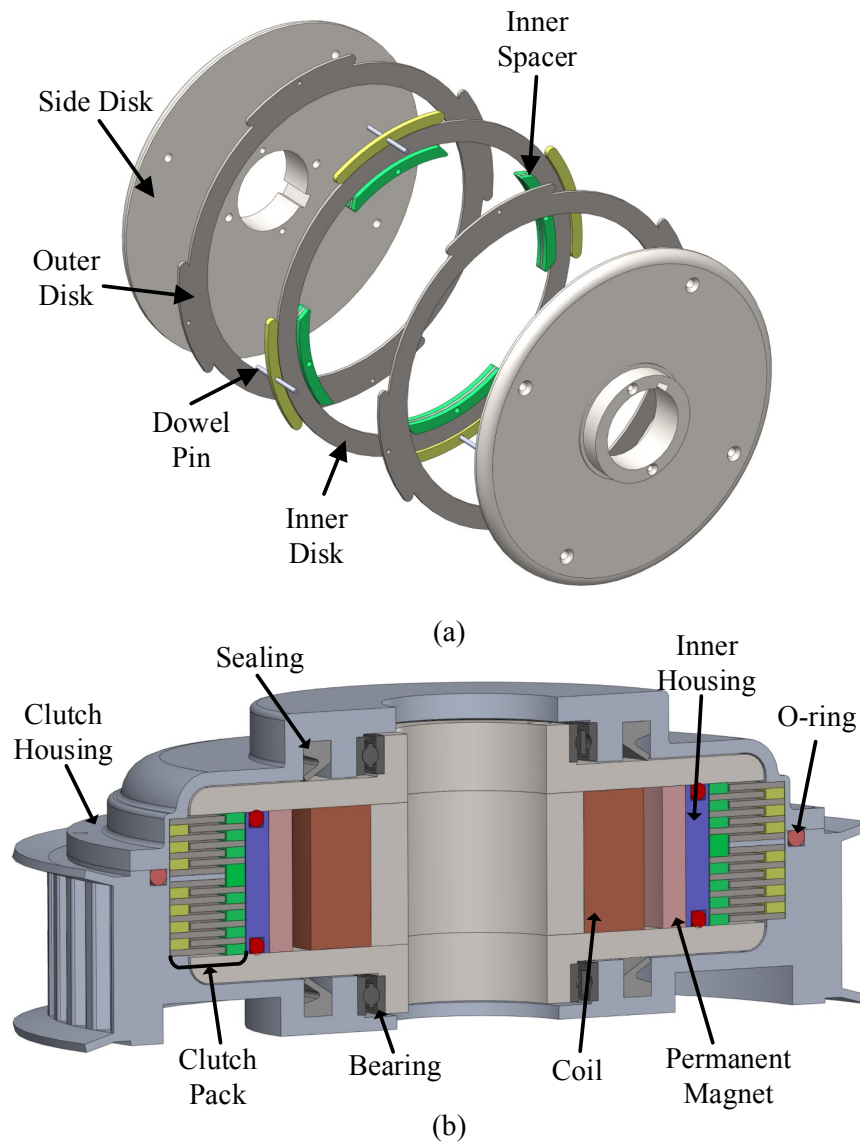


Figure 3.2: (a) Inner assembly of the clutch pack, (b) assembly of the HMR clutch.

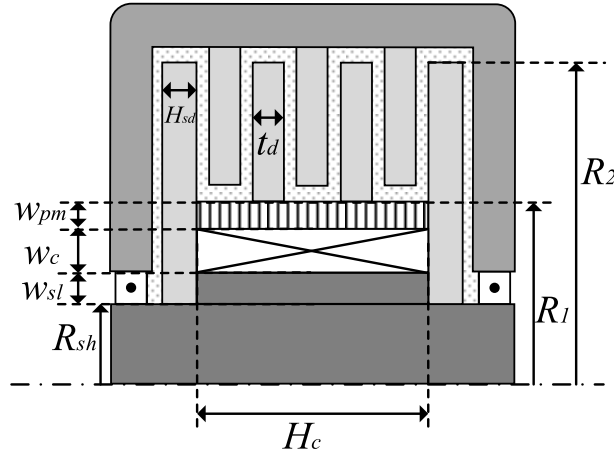


Figure 3.3: Geometry of the HMR clutch and its design parameters.

$$V_d = N\pi(t_d)(R_2^2 - R_1^2) \quad (3.11)$$

### 3.2.4 Finite Element Analysis and Optimization

In this section, the actuator is modeled and optimized using Finite Element Method (FEM). A 2D model of the HMR clutch is built to provide comprehensive information about the intensity of the (quasi-static) magnetic field inside the HMR clutch. This model also demonstrates the relationship between the input current and the magnetic field, and the output torque of the clutch. COMSOL Multiphysics® software is used as suitable platform to carry out the FEM simulations.

The optimization problem of a hybrid MR clutch based on the FEM based model is defined and solved in order to calculate the proper dimensions of the HMR clutch. Three main factors are considered in this optimization, namely the output torque (i.e.,  $f_1(x)$ ), total mass (i.e.,  $f_2(x)$ ), and magnetic field nullification of the clutch pack (i.e.,  $f_3(x)$ ). Each factor is a function of MR clutch dimensions, represented with the vector  $D$ .

The following objective function was used to obtain the optimal design parameters of the HMR clutch,

$$\begin{aligned} & \min |f_1(x) - \tau_d| \text{ and } \min f_2(x) \text{ and } \min f_3(x) \\ & \text{subject to } f(D) \end{aligned}$$

where  $\tau_d$  is the nominal output torque. A set of constraints  $f(D)$ , in the form of equalities and inequalities, are defined to meet the expectation of the design characteristic.

Table 3.1: Optimization Variable

Description	Variables	Lower limit	Upper limit	Optimized Value (rounded)
Bobbin width [mm]	$w_{sl}$	7	11	8
Disk width [mm]	$R_2 - R_1$	11	15	12
Side disk thickness [mm]	$H_{sd}$	4	7	5
Coil width [mm]	$W_c$	10	15	13.3
Permanent magnet Width [mm]	$W_{PM}$	3	7	5

1. the maximum current density due to coil temperature limitation (i.e.,  $\leq 2 \frac{A}{mm^2}$ )
2. physical relations between dimensions (e.g.,  $R_1 = R_{sh} + W_b + W_{coil} + W_{PM} + t_w$ ,  $R_2 > R_1$ )
3. availability of the material (e.g., standard steel sheets for disks, permanent magnet grade, bearings, etc)
4. minimum acceptable dimensions (e.g., minimum permanent magnet thickness, MR fluid gap, thickness of the inner housing)
5. radius of shaft is fixed to 15 mm.

Full factorial design is investigated to achieve MR clutches configurations in response of every possible combination of design parameters. Different ranges of optimization variables are studied to obtain the convergence ranges. Shortened ranges are defined in COMSOL Multiphysics® to conduct the local search optimization. Table 3.1 lists the optimization variables and the range considered for each variable.

Several tradeoffs exist in this problem. The shaft radius is fixed as it is supposed to be mounted on a DASA test bench to be paired with a conventional MR clutch. However, it is shown in [13] that unlike conventional MR clutches that the shaft is part of the magnetic circuit, HMR clutch is almost independent on the design on the shaft, therefore the radius of the shaft, and the total radius of the device could drop significantly in optimal HMR clutches. Since there is no single optimal solution for a multi-objective optimization problem, the solution space is, therefore, explored by inspecting a three-dimensional trade-off surface for the three design objectives. Fig. 3.4 shows all optimal solutions as a surface in three-dimensional space where



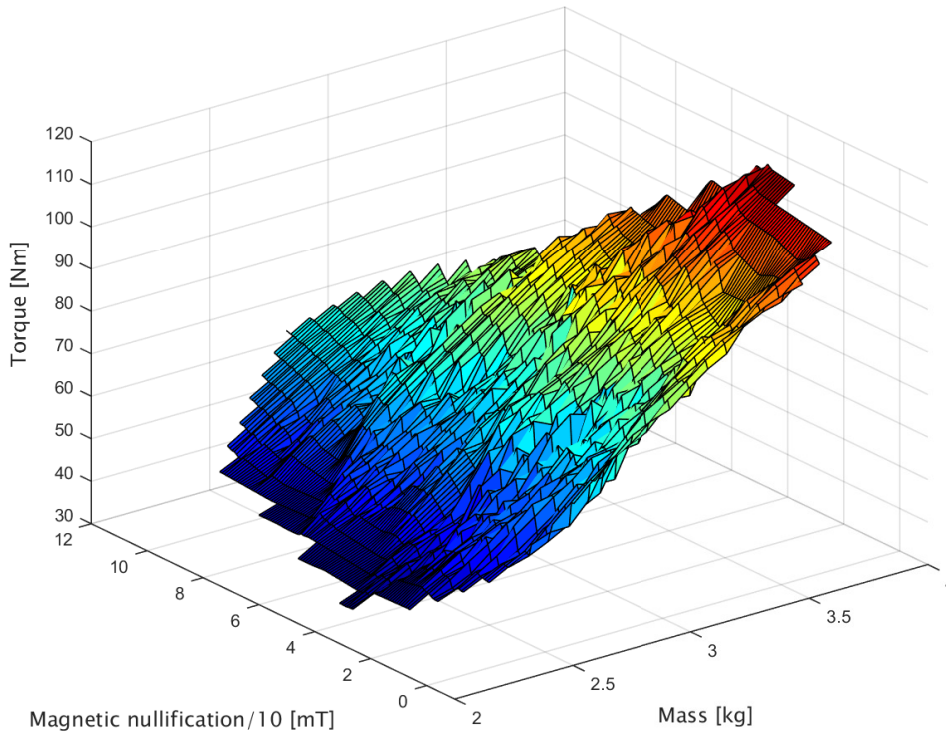


Figure 3.4: A trade-off surface in three-dimensional objective space.

the x axis is the mass, the y axis is the nullified magnetic field within the clutch pack, and the z axis is the maximum output torque. Fig. 3.4 shows that for a given mass, the output torque of the clutch is higher in designs that cannot necessarily nullify the magnetic field within the clutch pack, and those in the range of 40-60 mT.

Fig. 3.5 depicts the magnetic flux density contours inside the HMR clutch for different values of input currents between -2A and 4A corresponding to fully disengaged and fully engaged states of the clutch, respectively.

The strength of the permanent magnet inside HMR clutch has been selected such that the clutch can reach its minimum and maximum torques using optimal additional flux from the coil. As seen in Fig. 3.5(a), the coil can fully nullify the permanent magnet flux in the clutch pack, leading to fully disengage two parts of the clutch. The use of a permanent magnet changes the saturation point and helps the magnetic flux density to be distributed uniformly within the magnetic circuit. This configuration allows us to move the points along the magnetic circuit that are prone to saturation to other points within the circuit that are less exposed to the

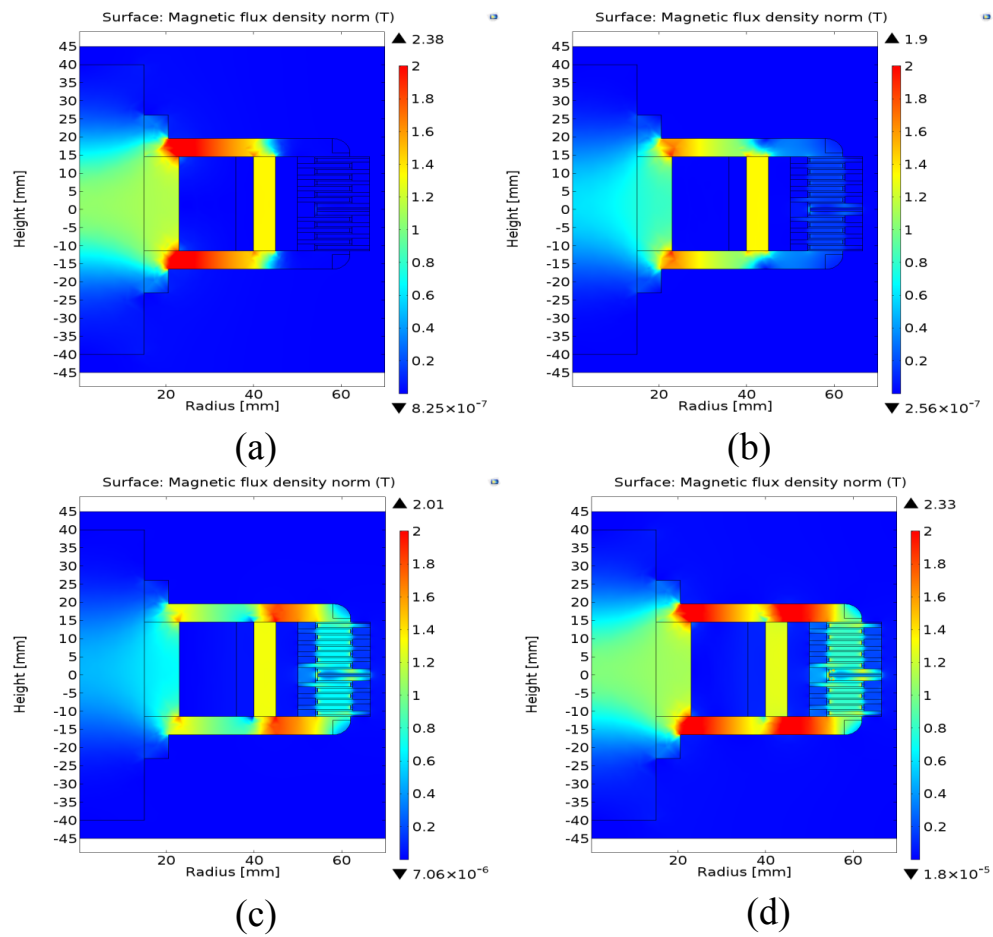


Figure 3.5: Magnetic flux density contour map in the Hybrid MR clutch when it is energized by (a) -2A, (b) 0A, (c) 2A, and (d) 4A.

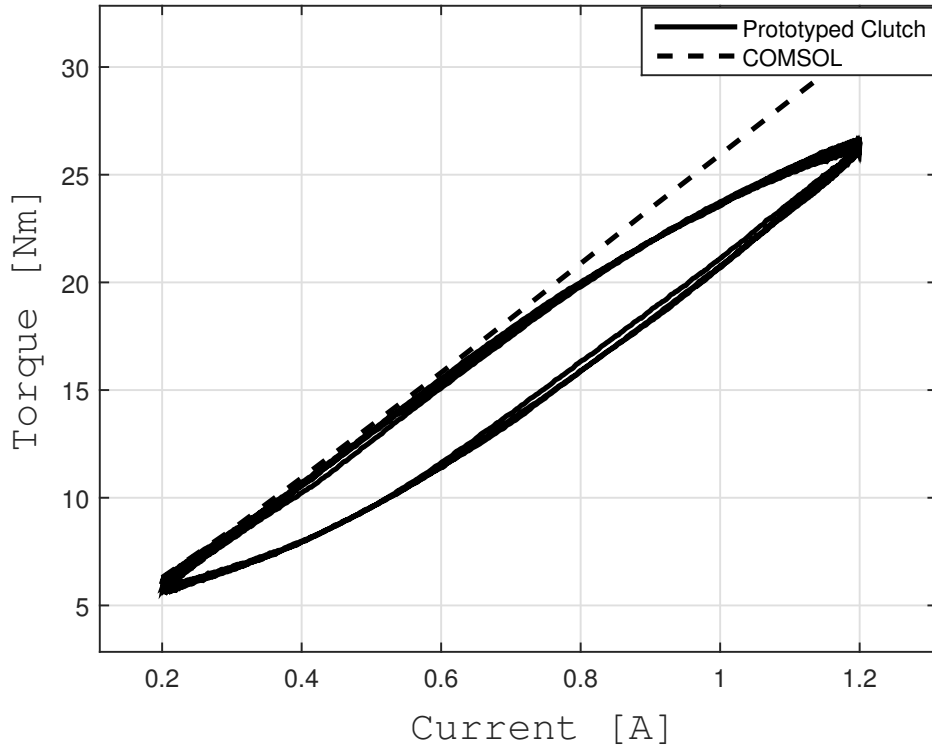


Figure 3.6: Comparison between measured results and simulation.

magnetic flux. In this way, the current density of the coil *ergo* the maximum torque of the HMR clutch can be increased before the magnetic circuit reaches the saturation. Put differently, for a given value of the current density the mass of the HMR clutch can be reduced by using less ferromagnetic materials in the magnetic circuit.

The transmitted torque of the HMR clutch is predicted using (3.3) and (3.4b) in our Finite Element model. In estimating the transmitted torque, the magnetic properties of the MR fluid used in the prototype, i.e., MRF-140CG, was included in the model. Although useful in providing insight into the design of the clutch, the model is not capable of representing the hysteretic behavior of the HMR clutches adequately. Fig. 3.6 depicts the transmitted torque of the prototype HMR clutch versus its applied current and compares the results with those predicted by the FEM based model. As observed, despite a close match between the data in the linear region of the graph, it is clear that the FEM base model is not able to capture and present hysteresis inside the HMR clutch.

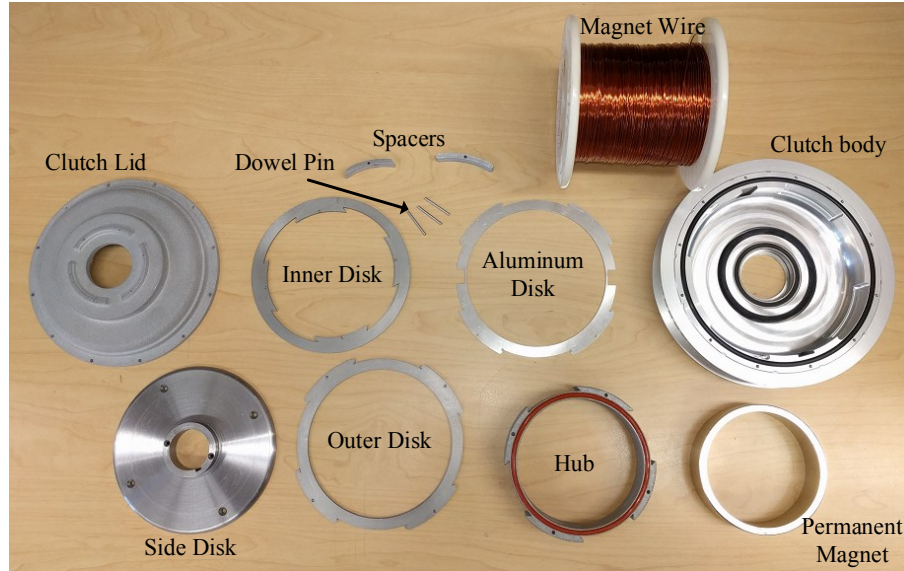


Figure 3.7: Components of the prototype hybrid MR clutch.

### 3.3 Prototype Hybrid MR clutch

A prototype HMR clutch using components shown in Fig. 3.7 was fabricated according to the proposed design.

Steel 1018 was selected for the shaft, bobbin, and the disks to direct the magnetic field. Laser cutting was used to cut the commercial quality GA18 steel sheet. The bobbin was coiled with a 21 gauge (i.e., American wire gauge) magnetic wire. Fibreglass resin was used to insulate the electromagnetic coil from MR fluid. A Neodymium permanent magnet ring (see Table 3.2) that was magnetized through its thickness was used inside the clutch pack. To protect the permanent magnet against corrosion, the magnet was coated with Nickel. Nonmagnetic materials were used to 3D print the required spacers in between the disks and clutch casing. To prevent leakage of the MR fluid, two sets of Teflon O-rings and seals were used inside the clutch. The specifications of the prototype HMR clutch are presented in Table 3.3. Table 3.4 presents the torque capacity and specification of the HMR clutch and the clutches developed for human-friendly robotic applications. This table also shows the torque capacity of the current research without using permanent magnet; i.e. if the electromagnetic coil was replaced by the combination of electromagnet and permanent magnet. The results show the superiority of the clutch in comparison to the state of the art.

Table 3.2: Configuration and properties of the permanent magnet

Type	Neodymium
Grade	N45
Remanence (Br) [kG]	1.33-1.38
Coerive Force (Hcb) [kA/m]	>756
Intrinsic Coercive Force (Hci) [kA/m]	>955
Max Working Temp. [C]	80
Inner diameter [mm]	80
Inner diameter [mm]	90
Width [mm]	26

## 3.4 Experimental Validation of the Prototype Hybrid MR Clutch

### 3.4.1 Experimental System

An experimental test bench (see Fig. 3.8) was used to evaluate the functionality of the HMR clutch. The test bench included a servo motor (Maxon EC 60) to provide the input torque to the HMR clutch. A high-power motor driver (Maxon Motors ADS 50/5 servo amplifier) set in current mode, provided the command current to the HMR clutch. A static load cell (Transducer Techniques SBO-1K) was employed to measure the output torque of the prototype clutch. An angular encoder (Renishaw RM22I) was employed to read the position of the output shaft. The HMR clutch included two analogue and two digital Hall sensors. Two unipolar ratio-metric analog Hall sensors (Infinion TLE4990) faced in opposite directions were used to measure  $\pm 400$  mT. Also, two bipolar digital Hall sensor (Infinion TLE4998S) were used to provide a measurement of  $\pm 200$  mT with a higher dynamic range. The Hall sensors were sandwiched in a pack of two steel disks and an aluminum disk in the centre. The aluminum disk was chosen for its similar reluctance to the Hall sensors and to allow magnetic flux density to distribute equally through the sandwich pack. A dSPACE (DS 1103, dSPACE Inc.) controller board was used to acquire the data at a sampling frequency of 500 Hz and to command suitable control signals to the actuator.

Table 3.3: Specifications of the hybrid MR clutch

Diameter [mm]	155
Width [mm]	59
MR fluid gap thickness [mm]	0.425
No. of input disks	8
Off-state torque [Nm]	4.5
Nominal torque (at 2 A) [Nm]	45
Maximum torque [Nm]	65
Total mass [kg]	3.1
Torque density [Nm/kg]	21

### 3.4.2 Current vs. Torque

To evaluate the performance of the prototype HMR clutch a series of tests were performed that are described in this section. Fig. 3.9 shows the block diagram of the system used to obtain the experimental results presented in this section.

#### Step Response

To evaluate the transient performance of the HMR clutch, the output torque of the clutch was obtained in response to a Step input current. To measure the output torque the input side of the clutch was driven at a constant mechanical speed while its output side was locked to a stationary load cell. The experimental result obtained using this test is shown in Figs. 3.10. In these figures, the solid line represent the measured output torque, the dash-dot line shows the decreed current, and the dash line shows the applied current by current driver. As observed, the output torque starts from a bias value of 4 Nm that is due to the use of permanent magnet. Also, the output torque has a relatively short rise time of about 40 ms, and 15 ms when the clutch is subjected to a step input current from 0 A to 1 A and 0 A to -1 A, respectively. One should note that this rise time is also partly due to the delay imposed by the electronics used to drive the clutch (i.e., Maxon ADS 50/5 servo amplifier).

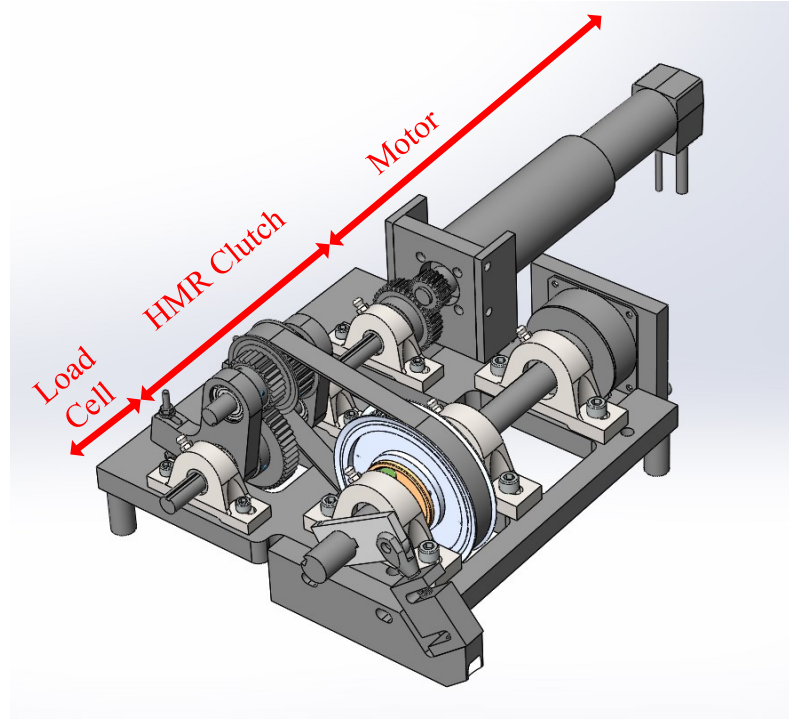


Figure 3.8: Experimental test bench for testing the prototype hybrid MR clutch.

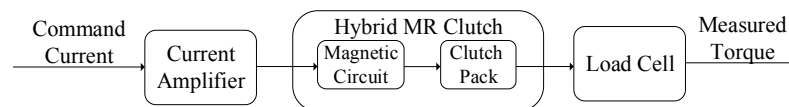


Figure 3.9: Block diagram of the frequency response experimentation.

Table 3.4: Comparison Between Prototype MR Clutches for Human-Friendly Actuator

Research	Torque [Nm]	Mass [Kg]	MRF gap[mm]	Number of disks
Current work	65	3.1	0.425	17
Current work w/o PM	36	3.4	0.425	17
Kikuchi et al. [14]	40	2.2	0.05	35
Shafer et al. [10]	75	4.5	0.5	18
Fauteux et al. [15]	11	2.4	NC*	NC*
Yadmellat et al. [8]	15	2.3	0.5	4

\* NC: Not clear

### Open-loop Frequency Response

To assess the performance of the HMR clutch in frequency domain, the open-loop frequency response of the clutch measured between the output torque of clutch and its input current was experimentally obtained. The frequency response was obtained by applying a sinusoidal (command) current with the amplitude of 0.5 A sweeping from 0.1Hz to 30 Hz to the clutch and measuring the corresponding output torque. The input part of the clutch was rotating at a constant speed while its output part was locked to a stationary load cell. The Bode diagram of the experimental results is shown in Fig. 3.11. As observed, the resulting 3-dB Open-loop bandwidth is measured to be approximately 20 Hz.

### 3.4.3 Torque Control Experiments

To evaluate closed-loop performance of the HMR clutch a PID controller was used to provide (command) current for HMR clutch in response to closed-loop feedback error between the desired and actual output torques. The PID controller was implemented on the dSAPCE DS 1103. Fig. 3.12 shows the closed-loop block diagram of the HMR clutch.



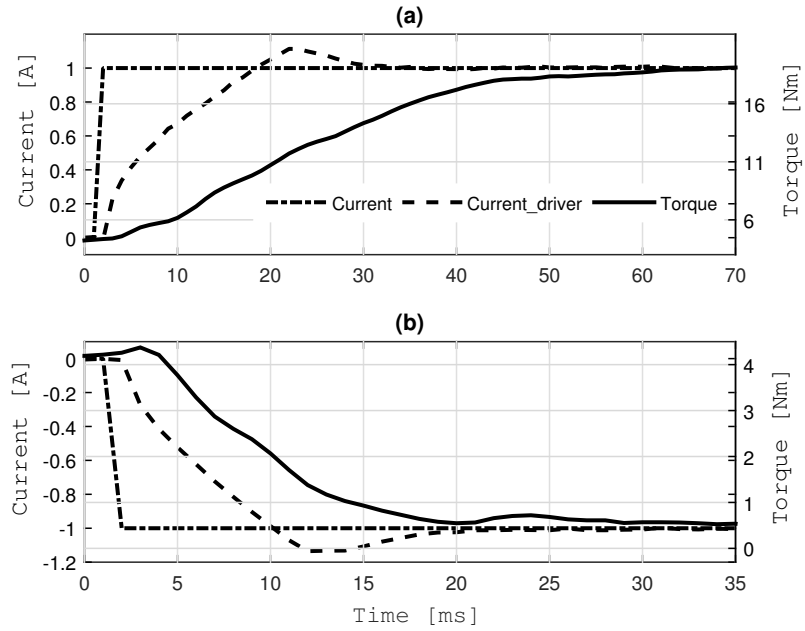


Figure 3.10: Evaluation of the transient performance of the HMR clutch when it is subjected to an input current (a) 0 A to 1 A, (b) 0 A to -1 A.

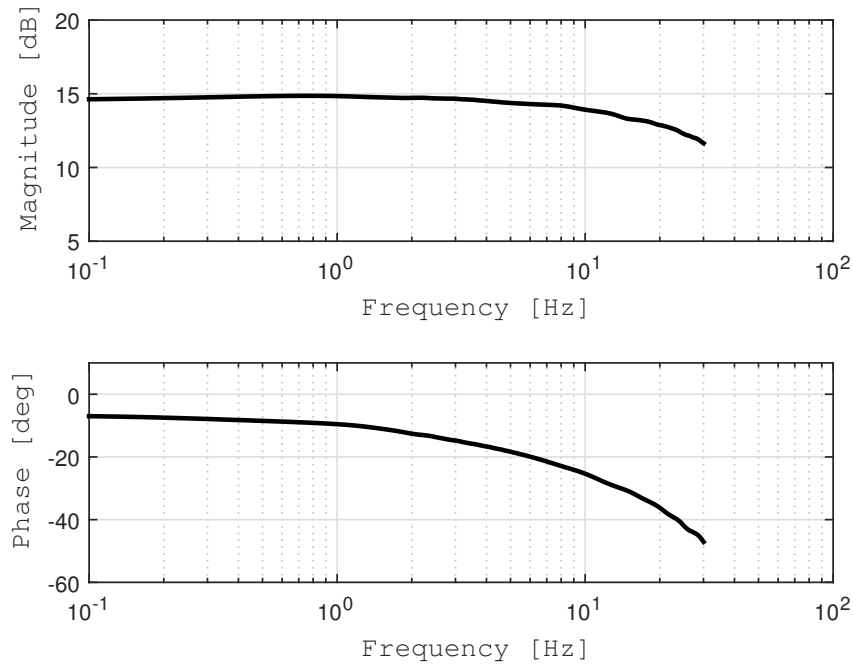


Figure 3.11: Open-loop frequency response.

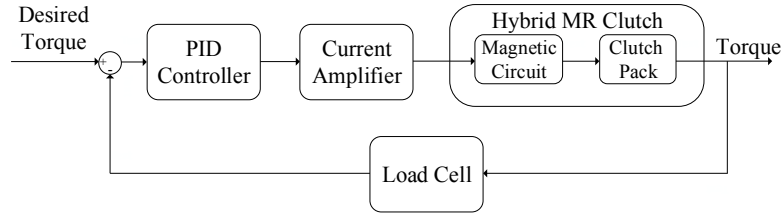
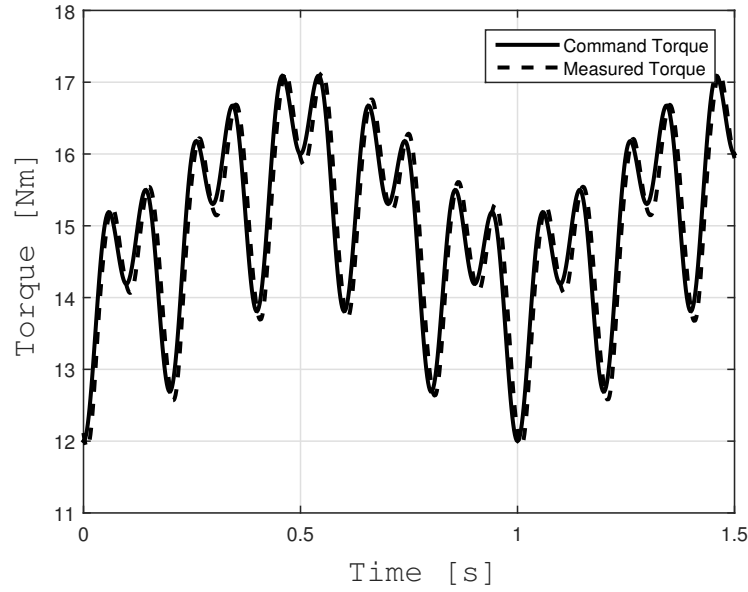


Figure 3.12: Closed-loop control block diagram

Figure 3.13: Torque tracking with  $T_d = \sin(2\pi t) + \sin(5 \times 2\pi t) + \sin(10 \times 2\pi t) + 15$ .

### Tracking of Desired Input

To assess the performance of the HMR clutch in time domain, a rapidly varying multi-sinusoidal signal was used as the desired torque value. The decreed torque included 3 sinusoidal signals with frequencies of 2, 5 and 10Hz and equal magnitude of 1Nm, as well as a DC component of 15Nm. Fig. 3.13 depicts the desired torque signal and compares it with the output torque of the clutch. As seen, the HMR clutch is capable of achieving fast and accurate torque tracking control.

### Frequency Response

The closed-loop frequency response of the HMR clutch was also studied. The closed-loop frequency response was obtained using a sinusoidal desired torque command sweeping from

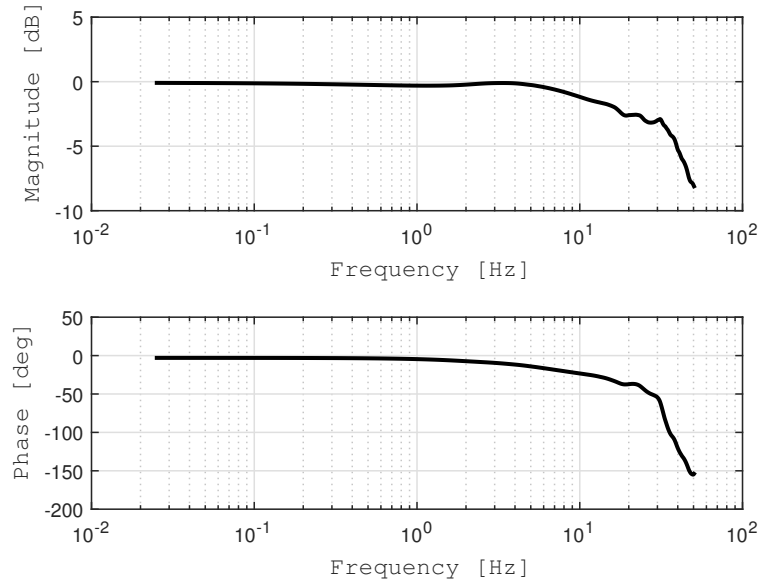


Figure 3.14: Closed loop frequency response of the prototyped HMR clutch.

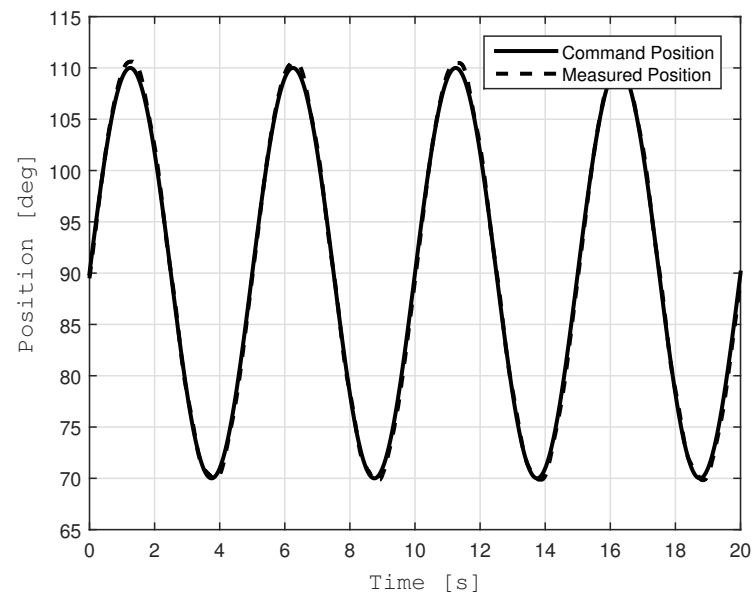
0 to 50 Hz and measuring the output torque. The input part of the clutch was rotating at a constant speed while its output part was locked to a stationary load cell. Fig. 3.14 illustrates the frequency response of the HMR clutch. As observed, using the 3-dB power loss cut-off frequency definition, the system bandwidth is measured to be approximately 30 Hz.

#### 3.4.4 Position Tracking Control Experiments

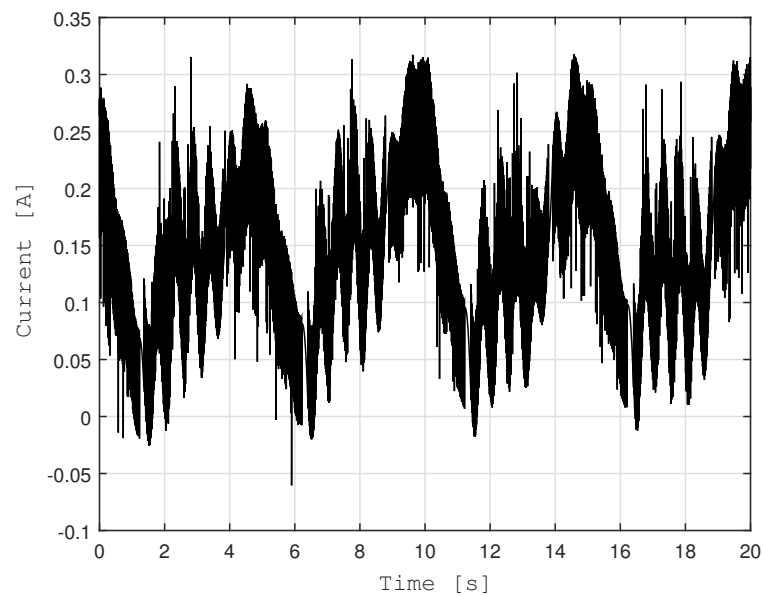
In this experiment, a 50-cm long arm constructed of medium density plastic was coupled to the output shaft. A counter weight of approximately 2 kg was mounted to the end of arm. The motor output was held at a constant rotational velocity. Position data was read from an encoder which monitors the output shaft. Figs. 3.15 and 3.16 show the response of this actuation paradigm to a sinusoidal input command ranging between  $70^\circ$  and  $110^\circ$ .

#### A-DASA motion control

The prototype HMR clutch was paired with a conventional MR clutch which was previously built in our research group to evaluate the efficacy of A-DASA using non analogous pair of clutches in delivering high performance motion control. Trajectory tracking experiments were

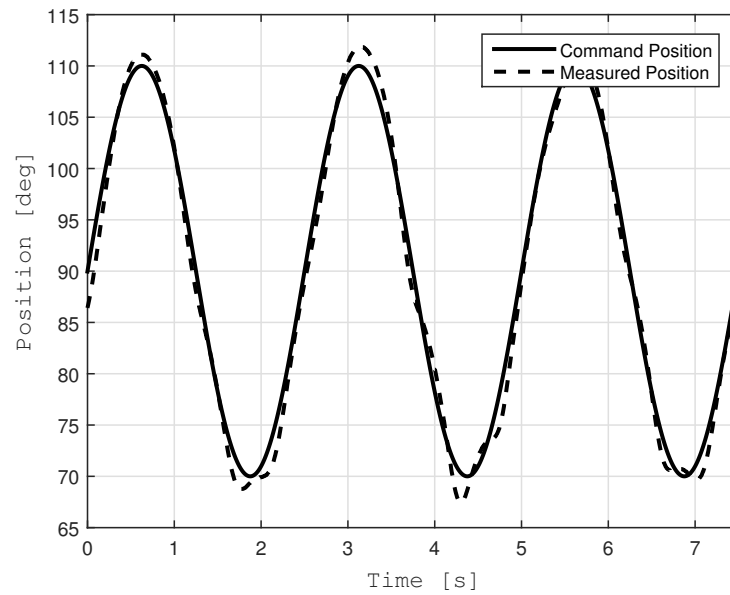


(a) Position control

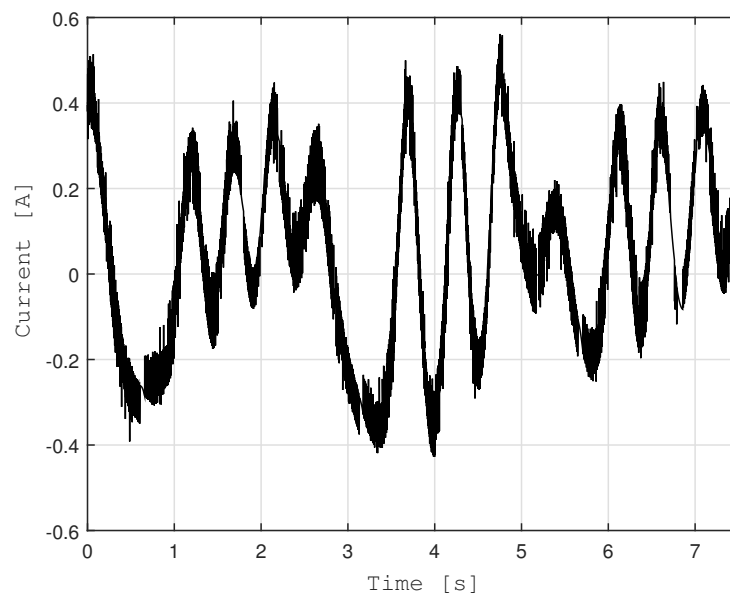


(b) Monitored current

Figure 3.15: Position tracking of sinusoidal input; period  $T = 5$  sec.



(a) Position control



(b) Monitored current

Figure 3.16: Position tracking of sinusoidal input; period  $T = 2.5$  sec.

conducted using the angular encoder to form the feedback signal. A 50-cm long arm constructed of medium density plastic was coupled to the output shaft. Fig. 3.17 and 3.18 show the response A-DASA actuation paradigm to a referenced position command. Fig. 3.18 indicates the capacity of the A-DASA actuators to achieve favorable precision in position control tasks. Fig. 3.19 depicts the result of the stabilization of this system when it is perturbed by external disturbances. As seen, a simple PID feedback controller and the back-drivable nature of this actuation system recover balance against external disturbances.

### **Repeatability**

In this section, the repeatability of the DASA actuation paradigm in force/torque and position control is studied. Ten experiments were performed to achieve the repeatability for each control mode.

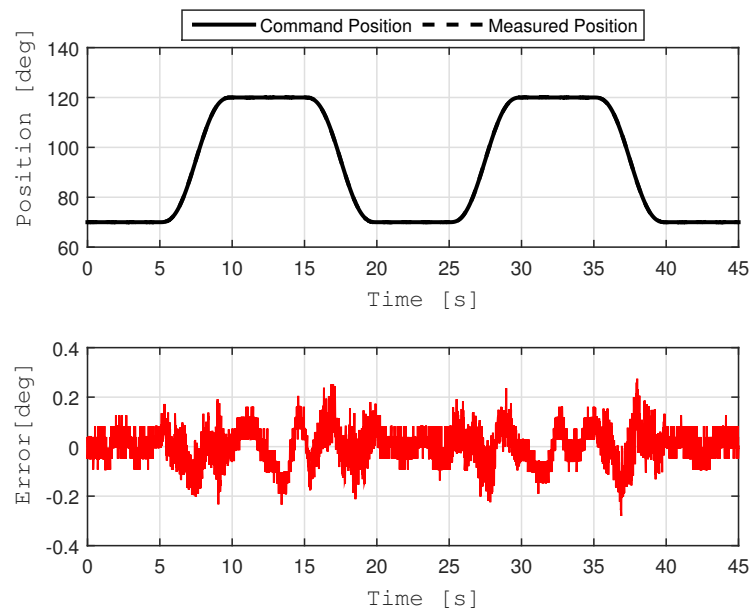
**Force/Torque Control;** In this set of experiments, the static load cell module was mounted to the test bench for closed loop torque control. A PID controller was used to develop the command signal. A step input from 0 Nm to 15 Nm at  $t=1$  sec was used as the desired torque value. The average of 3000 data upon achieving the desired constant torque 15 Nm was measured to obtain the repeatability of this experiment.

**Position Control;** In this set of experiments, the arm module was mounted to the test bench. Position data was read from the encoder which monitors the output shaft. A PID controller was used to develop the command signal. A step input from  $0^\circ$  to  $90^\circ$  at  $t=1$  sec was used as the desired position value. The average of 3000 data when the robotic arm reaches to the desired position  $90^\circ$  was measured to obtain the repeatability of this experiment.

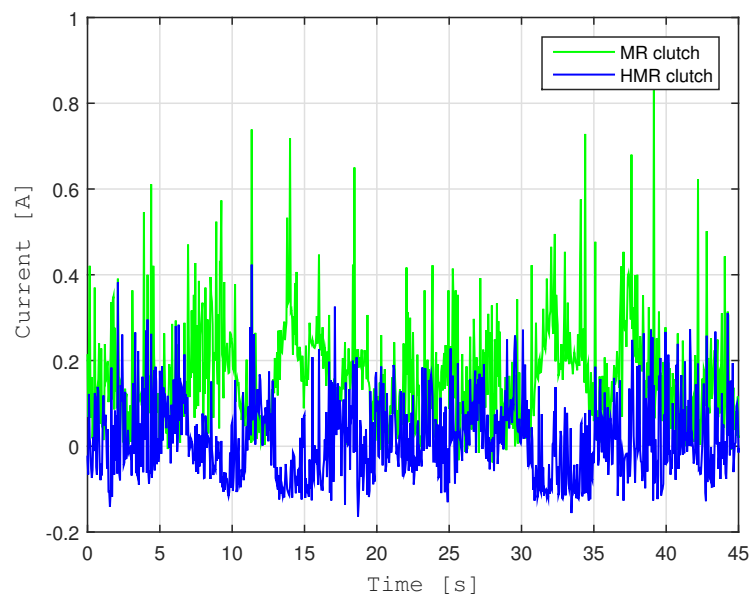
Fig. 3.20 and 3.21 show that the repeatability factors in force/torque and position are within the tolerance of 0.02 Nm and  $0.25^\circ$ , respectively.

## **3.5 Conclusions**

In this chapter the design and fabrication of a new HMR clutch was presented. The proposed HMR clutch utilized a combination of permanent magnet and electromagnetic coil for generating a magnetic field within the clutch pack. The use of a permanent magnet enabled us to reduce areas in the magnetic circuit that were prone to magnetic saturation. By decreasing saturations, one can increase the current density of the coil and the torque capacity of a HMR

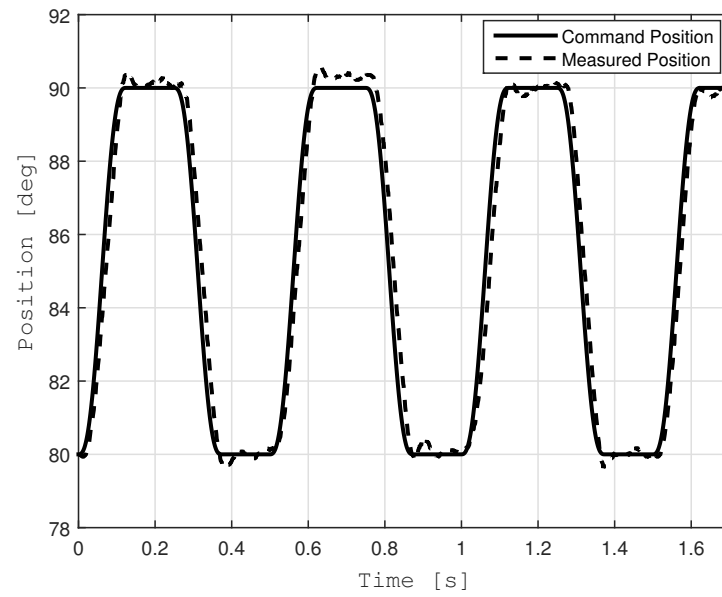


(a) Position control

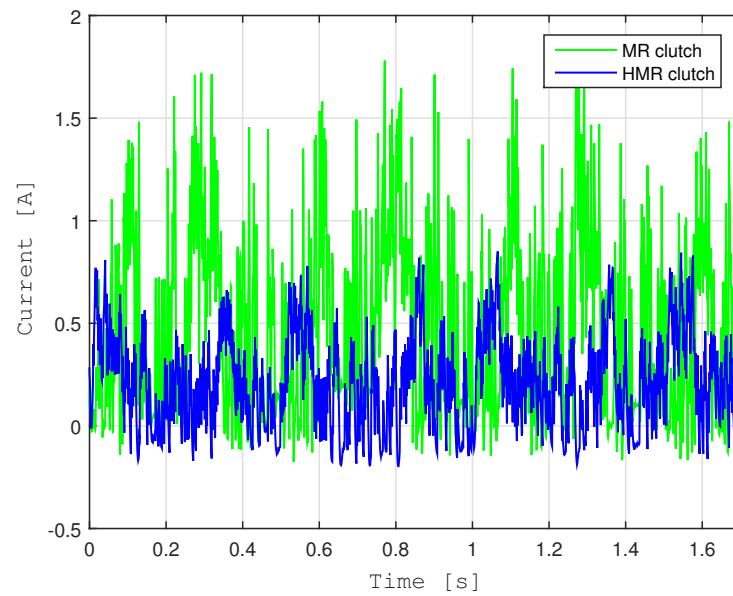


(b) Monitored current

Figure 3.17: A-DASA Position tracking result.



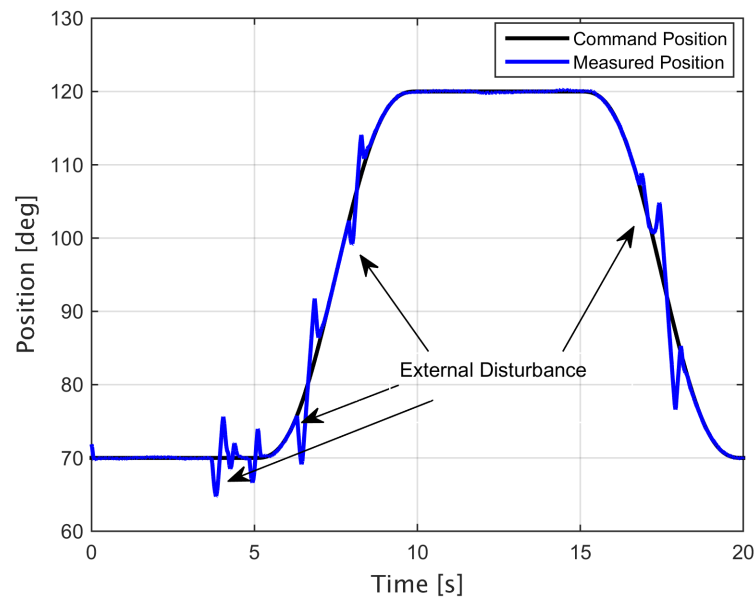
(a) Position control



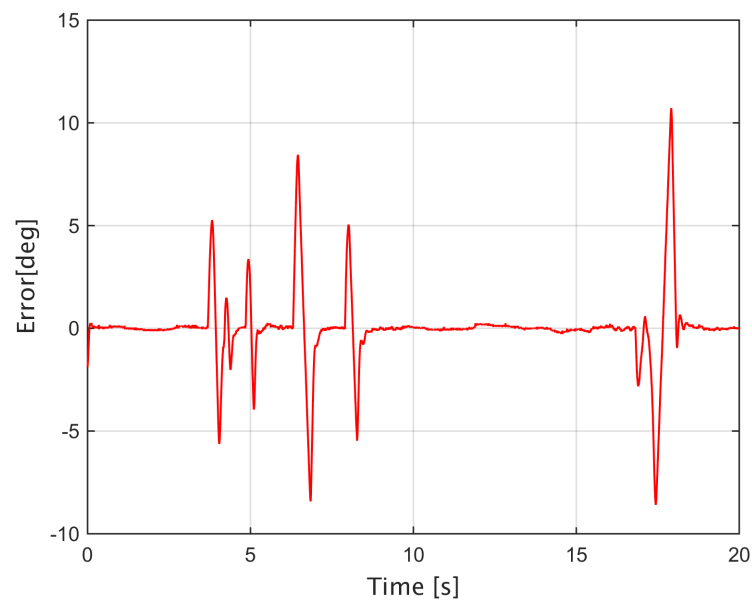
(b) Monitored current

Figure 3.18: A-DASA Position tracking result.





(a) Presence of external disturbance on A-DASA motion control



(b) Error

Figure 3.19: Presence of external disturbance on A-DASA motion control.

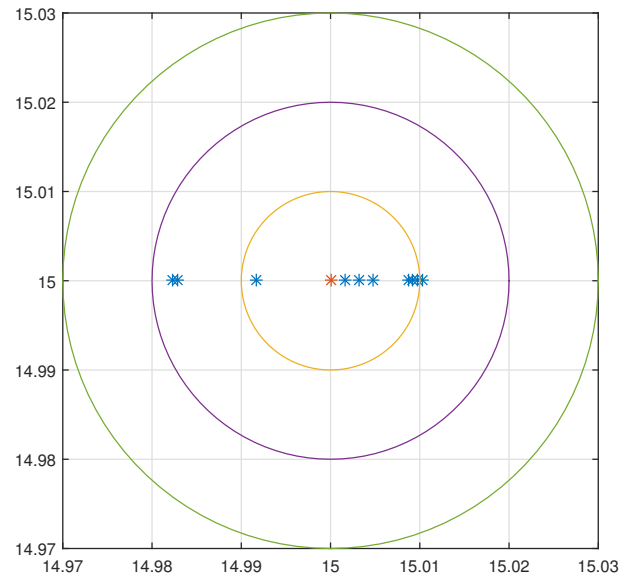


Figure 3.20: Repeatability in force/torque control.

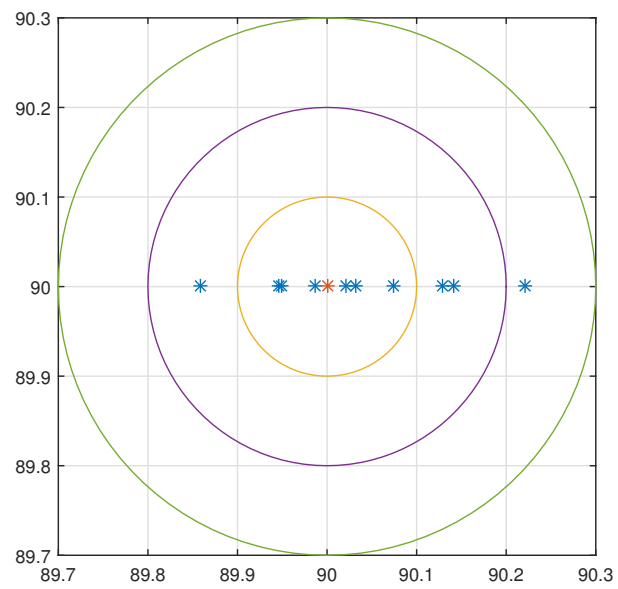


Figure 3.21: Repeatability in position control.

clutch. Stated differently, for a given nominal output torque, decreasing saturation allows to reduce the volume of material used in the magnetic path and the total mass of the clutch. Our previous results showed that a HMR clutch built in this way can have a torque-to-mass ratio of 40% higher than a conventional MR clutch. A prototype HMR clutch was designed, fabricated, and experimentally validated to further investigate the ability of the proposed design. The prototype HMR clutch has a maximum torque of 65 Nm and a mass of 3.1 Kg. The optimal light-weight design of the HMR clutches and inherently back-drivable nature of these devices make them an ideal candidate for human friendly robotic applications.

# Bibliography

- [1] M. Zinn, B. Roth, O. Khatib, and J. K. Salisbury, “A new actuation approach for human friendly robot design,” *The international journal of robotics research*, vol. 23, no. 4-5, pp. 379–398, 2004.
- [2] R. W. Armstrong, “Load to motor inertia mismatch: unveiling the truth,” in *Drives and Controls Conference*, 1998.
- [3] G. Pratt, M. M. Williamson, *et al.*, “Series elastic actuators,” in *Intelligent Robots and Systems 95. Human Robot Interaction and Cooperative Robots*, *Proceedings. 1995 IEEE/RSJ International Conference on*, vol. 1, pp. 399–406, IEEE, 1995.
- [4] G. Tonietti, R. Schiavi, and A. Bicchi, “Design and control of a variable stiffness actuator for safe and fast physical human/robot interaction,” in *Robotics and Automation, 2005. ICRA 2005. Proceedings of the 2005 IEEE International Conference on*, pp. 526–531, IEEE, 2005.
- [5] R. Schiavi, G. Grioli, S. Sen, and A. Bicchi, “Vsa-ii: a novel prototype of variable stiffness actuator for safe and performing robots interacting with humans,” in *Robotics and Automation, 2008. ICRA 2008. IEEE International Conference on*, pp. 2171–2176, IEEE, 2008.
- [6] M. Kermani and A. Shafer, “Magneto-and electro-rheological based actuators for human friendly manipulators,” Sept. 30 2014. US Patent App. 14/502,389.
- [7] A. S. Shafer and M. R. Kermani, “Development of high performance intrinsically safe 3-dof robot,” in *Robotics and Automation (ICRA), 2014 IEEE International Conference on*, pp. 619–624, IEEE, 2014.

- [8] P. Yadmellat, A. S. Shafer, and M. R. Kermani, "Design and development of a single-motor, two-dof, safe manipulator," *Mechatronics, IEEE/ASME Transactions on*, vol. 19, no. 4, pp. 1384–1391, 2014.
- [9] N. Takesue, J. Furusho, and M. Sakaguchi, "Improvement of response properties of mr-fluid actuator by torque feedback control," in *Robotics and Automation, 2001. Proceedings 2001 ICRA. IEEE International Conference on*, vol. 4, pp. 3825–3830, IEEE, 2001.
- [10] A. S. Shafer and M. R. Kermani, "On the feasibility and suitability of mr fluid clutches in human-friendly manipulators," *Mechatronics, IEEE/ASME Transactions on*, vol. 16, no. 6, pp. 1073–1082, 2011.
- [11] R. W. Phillips, *Engineering applications of fluids with a variable yield stress*. PhD thesis, University of California, Berkeley, 1969.
- [12] J. D. Carlson, "Mr fluids and devices in the real world," *International Journal of Modern Physics B*, vol. 19, no. 07n09, pp. 1463–1470, 2005.
- [13] M. Moghani and M. R. Kermani, "Design and development of a hybrid magnetorheological clutch for safe robotic applications," in *Robotics and Automation (ICRA), 2016 IEEE International Conference on*, IEEE, 2016.
- [14] T. Kikuchi, K. Otsuki, J. Furusho, H. Abe, J. Noma, M. Naito, and N. Lauzier, "Development of a compact magnetorheological fluid clutch for human-friendly actuator," *Advanced Robotics*, vol. 24, no. 10, pp. 1489–1502, 2010.
- [15] P. Fauteux, M. Lauria, B. Heintz, and F. Michaud, "Dual-differential rheological actuator for high-performance physical robotic interaction," *Robotics, IEEE Transactions on*, vol. 26, no. 4, pp. 607–618, 2010.

## Chapter 4

# Hysteresis Modeling of a Hybrid Magneto-Rheological Actuator

*The material presented in this chapter is published in the proceeding of "IEEE/ASME International Conference on Advanced Intelligent Mechatronics," Banff, Alberta, Canada, 2016.*

A hybrid MR clutch utilizes a permanent magnet and an electromagnetic coil to generate the magnetic field within the clutch pack. The existence of nonlinear hysteretic behavior between the input and output of the MR clutches needs to be fully investigated in order to perform high fidelity force/torque control. In this paper, a closed-loop torque control strategy is presented. The feedback signal used in the closed-loop control is estimated using an Artificial Neural Network (ANN) that uses magnetic field measurements from an embedded Hall sensor inside the clutch. The developed neural network is capable of accurately predicting the transmitted torque as well as modeling the hysteretic relationship between the applied current, internal magnetic field within the clutch, and the output torque of the actuator. This technique introduces a cost effective force/torque control by eliminating the need for conventional torque sensors for providing feedback. The performance of the trained neural network and the said control strategy are experimentally validated. The results clearly show the ability of a hybrid MR clutch in delivering torque tracking control with high fidelity required in many human-safe actuation systems.

## 4.1 Introduction

In recent years, considerable attentions have been given to the field of the physical human robot interactions (pHRI). A particular subject of interest in these considerations is the safety of humans within the interactive environments. This has led to the design and development of several new actuation concepts that are naturally compliant and have low impedance. Compliant actuators are meant to disengage the reflected inertia of the actuator (through reduction gears) from the actuator load. Series elastic actuator (SEA) [1] was an initial attempt to reduce the actuator's impedance using an elastic element placed between the motor and its load. This concept required a trade-off between safety characteristics of the actuator and its performance, resulting in limited controllable bandwidths. Distributed macro-mini actuation (DM<sup>2</sup>) [2] was introduced later to maintain the inherent safety, while preserving performance. DM<sup>2</sup> actuation approach utilizes a parallel combination of low and high frequency actuators. In this concept, low-frequency high-torque actuators are used to do the “heavy-lifting jobs”, while the high-frequency torque actuation is maintained using small motors. For the high-frequency actuation, very low impedance is achieved by connecting the motor to the manipulator through low-friction, low-reduction cable transmissions. As for low frequencies, low impedance is achieved using series elastic actuators (SEA). Such systems increase both mechanical and control complexities of the actuation mechanism.

A new actuation concept called Distributed Active Semi-Active Actuation (DASA) [3] was introduced by our research group for human-safe robotic applications. In this concept, the entire actuation mechanism for the system is treated as one unit that includes one active component (e.g. an electric motor) as a source of mechanical energy and a set of semi-active components, i.e., Magneto-Rheological (MR) clutches, for distributing the mechanical energy of the source to various loads (e.g. robot links) in the system. MR clutches replace the reflected inertia of the actuator with the low inertia of the clutch itself [4]. Since there is no hard coupling between the input and output, an MR clutch (hence DASA) offers inherent compliance and with minimal output inertia. Other inherent attributes of DASA such as high torque-to-mass, high torque-to-inertia, and high bandwidth provide the prerequisite requirements of intrinsic safe actuation while maintaining the dynamical performance of the actuator.

One difficulty in employing MR clutches in DASA actuation is the nonlinear behavior between the input and output of the actuator. Both ferromagnetic material used inside an MR

clutch and MR fluid itself introduce nonlinearities that make the modeling and control of this family of actuators challenging, although MR fluids exhibit little hysteresis in comparison to ferromagnetic materials [5]. The Bingham visco-plastic model [6] is widely used to relate the shear stress of the MR fluid to an applied magnetic field. This model ignores the nonlinearities of the fluid due to hysteresis, but is sufficiently adequate for the design and analysis of MR clutches in most applications. Other models that do not ignore nonlinear behaviors of MR fluids, such as Herschel-Bulkley model [7], and Bouc-Wen model [8] are complex and do not offer significant advantages for most common applications of MR clutches. Hence, in most studies the main emphasis of the modeling is on the hysteresis of the ferromagnetic materials. A widely used hysteresis model for ferromagnetic materials is the Preisach model [9]. The challenges of obtaining an inverse of the Preisach model restrict the utilization of this model in real-time control applications. Prandtl-Ishlinskii [10] and Krasnoselskii-Pokrovskii [11] models are also among others hysteresis modeling approaches that require complex implementations with limited use in real-time closed-loop control applications [12].

The main contribution of this work is to evaluate the use of an Artificial Neural Network (ANN) for modeling and control of the hybrid MR actuator. The ANN is trained using a large set of pre-recorded experiments to estimate the hysteretic nonlinear behavior between the applied current and transmitted torque of the MR clutch. This model is then used to provide closed-loop feedback for force/torque tracking control. The novelty of this model is to eliminate the need of force/torque sensor in the actuation mechanism. The performance of the hybrid MR clutch and the effectiveness of the proposed model are experimentally validated and the results are compared with those obtained from a torque sensor.

The remaining of this chapter is organized as follow: Section 4.2 briefly introduces the structure of a hybrid MR actuator prototype. Section 4.3 presents the process of training of the ANN using measured data. Section 4.4 demonstrates experimental results for force/torque tracking control using the developed ANN and compares the estimated results with those acquired from an actual torque sensor. Finally, Section 4.5 concludes the paper and addresses future works.



## 4.2 Hybrid MR Actuator

In the late 1940, Magneto-Rheological (MR) fluids were discovered as materials with ability to change their shear strength within few milliseconds in response to external magnetic fields [13]. MR fluids are typically made from water or oil carrying suspended micron-sized particles. The viscosity of the fluid can be controlled with an external magnetic field through the formation of particles into columns aligned in the direction of the field. The use of MR fluids has been extended into compliant actuation mechanisms in that a clutch-like device filled with MR fluids, hence the name MR clutch, is used as the complaint element. MR clutches have the capability of transmitting input mechanical power to their output in proportion to the intensity of an applied magnetic field. In a Hybrid MR clutch (HMR clutch), a combination of a permanent magnet and an electromagnetic coil is used to develop the required magnetic field [14]. Fig. 4.1 depicts a cross-section of a HMR clutch along with the magnetic field distribution inside the clutch. The HMR clutch consists of an interchanging stack of input and output disks arranged around the rotational axis of the clutch with the space between them filled with MR fluid. As shown in Fig. 4.1 A, the magnetic fields generated by the permanent magnet crosses the MR fluid and sets the MR fluids resulting in partial torque generation in the HMR clutch. An electromagnetic coil is used to adjust the output torque by tuning the magnetic field strength. Fig. 4.1 B and C depict two boundary cases where the applied current to the electromagnetic coil results in the maximum and minimum, i.e., absolute zero, output torque in the HMR clutch, respectively. One can note that the electromagnetic coil is arranged such that its magnetic flux either adds or completely negates the flux of the permanent magnet and its hysteresis remanence (depending on the polarity of the current) within the MR fluids.

### 4.2.1 Prototype Hybrid MR clutch

To investigate the characteristics of the proposed HMR clutch, a prototype as shown in Fig. 4.2 was designed, developed, and fabricated. This design is composed of input/output magnetic disks that are held apart with non-magnetic spacers. The inner disks are mechanically coupled to the shaft, while the outer disks are fixed to the clutch casing. A permanent magnet ring is integrated inside the HMR clutch to produce a bias electromagnetic flux. N45 Neodymium magnet was chosen during optimization process to allow achieving absolute zero and maximum torques using minimal magnetic flux supplements from the electromagnetic coil. When the

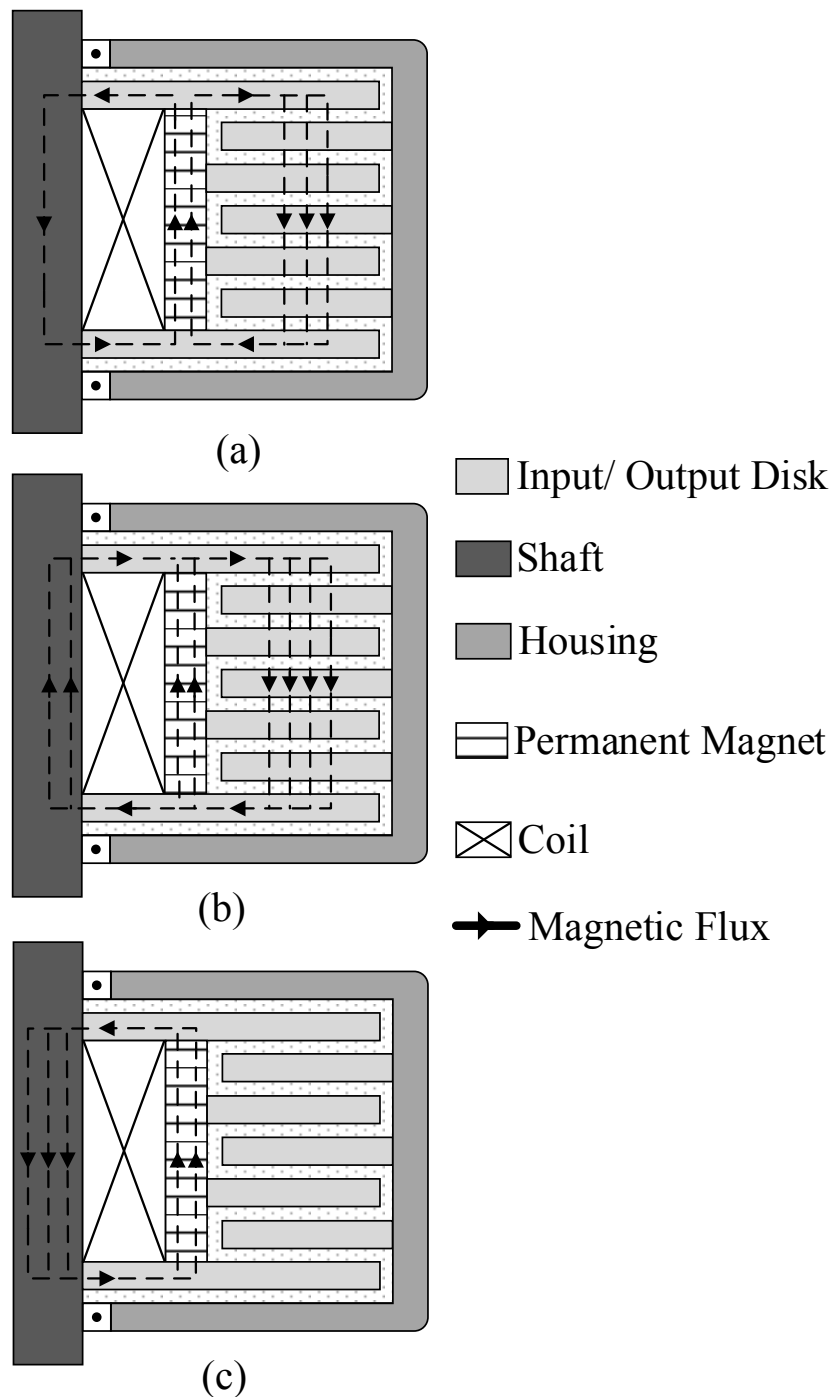


Figure 4.1: Magnetic field distribution inside a hybrid MR clutch: (a) magnetic flux density ( $B$  field) distribution inside the MR clutch due to the permanent magnet (off-state), (b) the field enhancement in the MR clutch pack with an applied magnetic field, and (c) the field cancellation in the MR clutch pack due to an applied magnetic field in reverse direction.

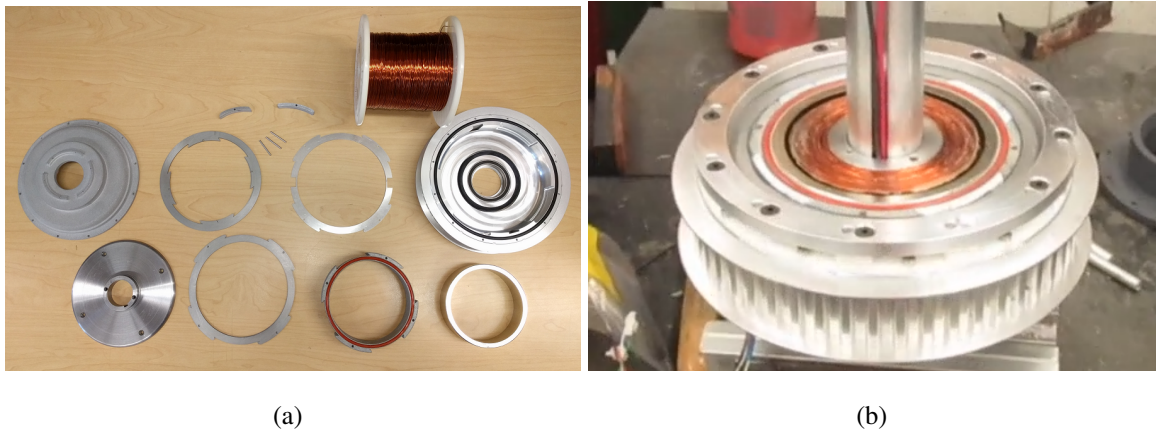


Figure 4.2: Prototype of the hybrid MR clutch. (a) Components of the prototype. (b) Assembly of the prototype.

electromagnetic coil is energized (depending on the polarity of the applied current), the shear stress of the MR fluid is altered (increased or decreased) within the magnetic path, allowing the HMR clutch to fully transmit or disengage the input mechanical power. Using this combination much higher torque-to-mass ratios can be obtained in comparison to coil-based MR clutch. The specifications of the prototype HMR clutch are presented in Table 4.1.

### 4.2.2 Integration of the Magnetic Sensor

The location of the magnetic sensors should be carefully chosen to accurate measurement of the magnetic flux inside the clutch. The flat surface of the magnetic sensor (Hall sensor) should be perpendicular to the path of the magnetic field to measure both the direction and magnitude of the flux. Given their comparable permeability to air, magnetic sensors must be placed in a location within the magnetic path that forces the magnetic flux to pass through the sensors. Fig. 4.3 shows the locations of the magnetic (Hall) sensors inside the prototype HMR clutch. The Hall sensors are sandwiched in a pack of two steel disks and an aluminum disk. The aluminum disk is chosen for its similar reluctance to the Hall sensors, allowing the magnetic flux density to be distributed equally through the sandwich pack. The clutch is designed to integrate two analogue and two digital Hall sensor assemblies. Two unipolar ratio-metric analog Hall sensors (Infinition TLE4990) faced in opposite directions were used to measure  $\pm 400$  mT. Also, two bipolar digital Hall sensors (Infinition TLE4998S) were integrated inside the clutch to measure  $\pm 200$  mT. The digital sensors provide a Single Edge Nibble Transmission (SENT) signal based

Table 4.1: Specifications of the Hybrid MR Clutch

Diameter [mm]	155
Width [mm]	59
MR fluid gap thickness [mm]	0.425
No. of input disks	8
Off-state torque [Nm]	4.5
Nominal torque(at 2 A) [Nm]	45
Maximum torque [Nm]	65
Total mass [kg]	3.1
Torque density [Nm/kg]	21

on the SAE J2716 standard [15], which consists of a sequence of pulses. Each transmission has a constant number of nibbles containing the flux value, the temperature, and status information of the sensor. These digital sensors are used to monitor the magnetic field and temperature of the MR fluid simultaneously.

### 4.3 Modeling and Control of Hybrid MR Actuator

HMR clutches, being a ferromagnetic based device, suffer from a nonlinear hysteresis relationship between the input current of the clutch and the output torque transmitted through the clutch [16]. In order to characterize this behavior of the HMR clutches, input-output measurements using sinusoidal input current with three different frequencies were used. A set of experimental data for three frequencies of 1 Hz, 4 Hz, and 8 Hz is shown in Fig. 4.4. This figure illustrates the hysteretic behavior between the applied current, internal magnetic field, and the output torque of the HMR clutch. The results also show that the hysteresis is a rate dependent characteristic that can change with frequency.

The results also ascertain the necessity of investigating an accurate modeling technique of HMR actuators for reliable force/torque control. Obviously, employing a conventional force/torque sensor used in a closed-loop feedback configuration to regulate the torque is an option. However, these sensors are notoriously famous for having high level of noise. Moreover,

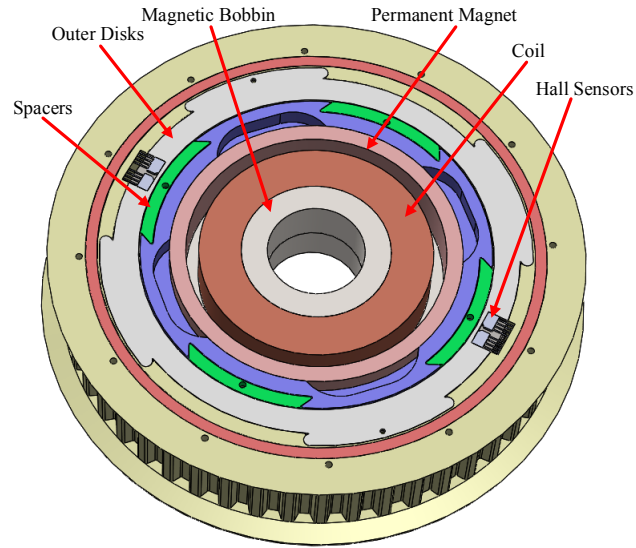


Figure 4.3: Location of hall sensors inside the hybrid MR clutch.

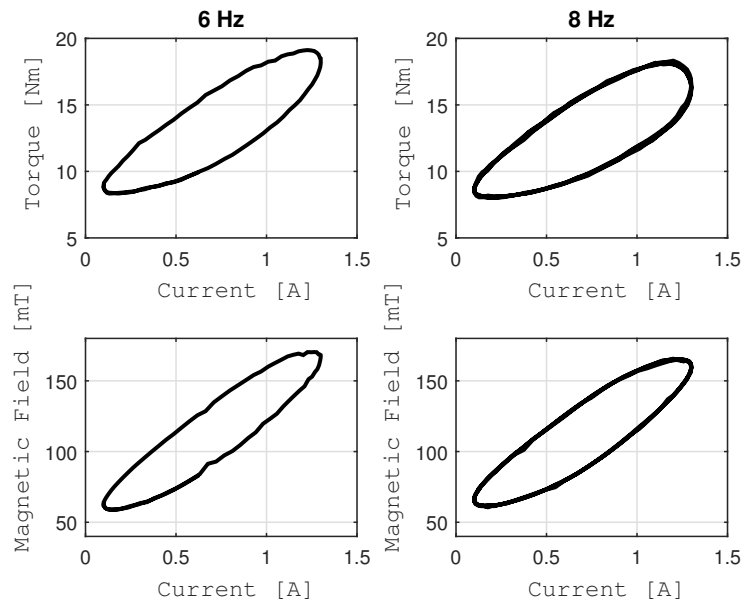


Figure 4.4: Hysteretic behavior for an MR clutch.

these sensors are often used in a non-collocated configuration making them prone to friction, backlash and additional noises. Finally, in applications such as robotics in which task space forces/torques of the robot end point are related to joint space torques of each joint using Jacobean matrix achieving force/torque control with high fidelity is even more difficult. It is due to these reasons that it becomes highly desirable to study and deal with nonlinear behavior of HMR clutches, mainly hysteresis, to obtain an alternative solution to conventional force/torque sensors. To this effect, magnetic field measurement from within the clutch pack is used as the feedback signal to estimate the transmitted torque and to compensate for the hysteresis between the input current and the magnetic field. One should also note that since magnetic field measurement is collocated with the actuator, the measurement will not be susceptible to any of the issues raised with conventional force/torque sensors. Next, an Artificial Neural Network (ANN) is considered to peruse the input-output relationship of the HMR clutch.

### 4.3.1 Artificial Neural network

Artificial neural networks (ANNs) have been widely used in nonlinear hysteresis modeling and control [17–22]. This interest is due to their high capability in learning and adaptation. ANNs show much better performance than standard mapping techniques in the presence of hysteresis, noise, and other nonlinearities in time series. Among the reasons are the ability of ANNs to learn from actual experimental data and the intrinsic nonlinearity of ANN models. A feed-forward neural network with a hidden layer [23] is considered for studying the hysteretic behavior of a HMR clutch. Fig. 4.5 shows the architecture of a feed-forward neural network. A nonlinear autoregressive network with exogenous inputs (NARX) is considered, i.e.,

$$y(t) = F(x(t-1), \dots, x(t-d), y(t-1), \dots, y(t-d))$$

where  $F$  is a nonlinear function of its arguments,  $x$  is the input,  $y$  is the predicted output, and  $d$  is the number of previous samples in the data set. Modeling the nonlinear behavior of the clutch is based on training the NARX network from the actual sets of data acquired from magnetic and torque sensors.

To generate the training data sets, different input currents were applied to the prototype clutch and the corresponding internal magnetic field and the output torque were recorded. In order to increase the accuracy of the network, several input currents including sinusoidal with different magnitudes and frequencies, swept sine chirps, and steps were applied. The neural

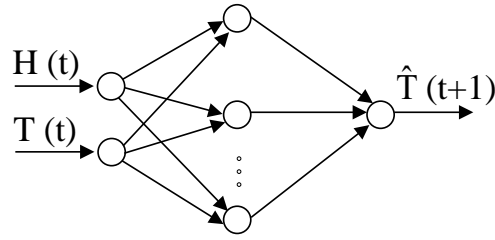


Figure 4.5: Architecture of the feed-forward neural network.

network was then trained based on the known internal magnetic field and the transmitted torque. The Neural Network Toolbox in MATLAB® was used to train the neural network with this set of data using the Levenberg-Marquardt algorithm. In this algorithm. The number of hidden neurons and the delay memory lines were chosen as 20 and 8 by trial and error, respectively.

### 4.3.2 Torque Control Scheme

The main notion behind “sensor-less” force/torque tracking control of a HMR clutch is the one-to-one relation between the internal magnetic field and the output torque. This relationship is shown in Fig. 4.6 when the clutch is subjected to a sinusoidal input current with different frequencies. This relationship allows controlling the torque of the hybrid MR clutch precisely in a configuration shown in Fig. 4.7 which depicts a closed-loop torque control strategy for a HMR clutch using a simple PID controller and a trained ANN. The error is formed by comparing the desired output torque and its estimated values. The estimated value of the output torque is obtained using the trained network as described in the previous section. The PID controller provides a reference signal for a current driver that drives the electromagnetic coil inside the HMR clutch to add to or subtract from the bias magnetic field of the permanent magnet. In the next section, we show the results for performance evaluation of this system.

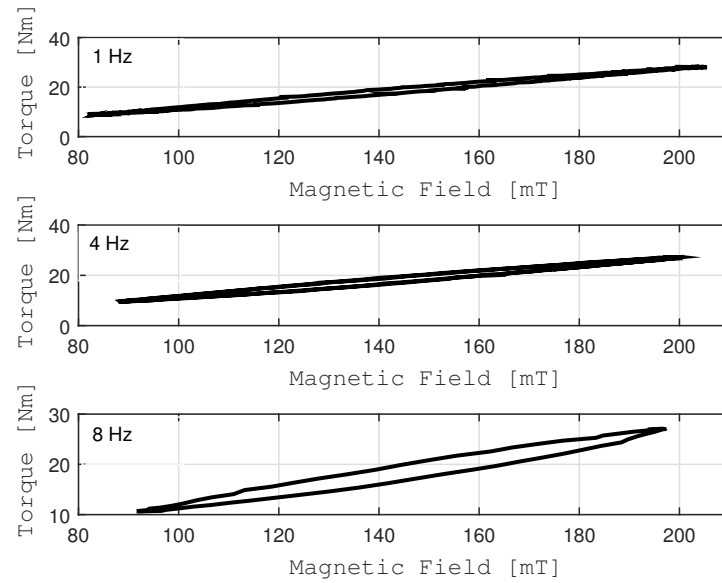


Figure 4.6: Output torque versus magnetic field.

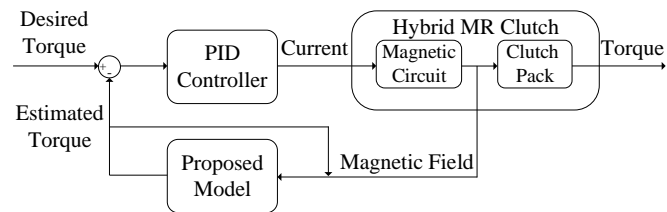


Figure 4.7: Closed-loop control configuration using embedded Hall sensors.



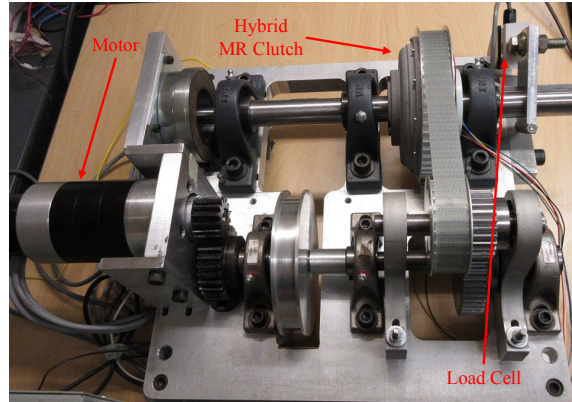


Figure 4.8: Experimental test bench.

## 4.4 Experimental Results

### 4.4.1 Experimental Test Bench

To acquire the torque transmitted by the HMR clutch in different working conditions and to compare the estimated torque of the ANN to those obtained using actual measurements, the prototype HMR clutch was mounted on an experimental setup shown in Fig. 4.8. A servo motor (Maxon EC 60) provides the rotational inputs to the HMR clutch. A servo amplifier (Maxon 4-Q-DC Servo-amplifier ADS 50/5), set in torque mode, is used to control the current to the MR clutch. Two unipolar ratio-metric Hall sensors (Infinion TLE4990) embedded in the HMR clutch and faced in opposite directions measure the strength of the magnetic field up to  $\pm 400$  mT. A static load cell (Transducer Techniques SBO-1K) is employed to measure the output torque of the prototype clutch. A dSPACE controller board (DS 1103, dSPACE Inc) is used to acquire the data at a sampling frequency of 500 Hz and to generate suitable control signal commands for the HMR clutch.

### 4.4.2 Validation of the Modeling Method

In this section, the results from several experiments to validate the accuracy of the trained network are presented. These results were obtained to assess the ability of the ANN in predicting nonlinear characteristics of a HMR clutch. Two sinusoidal input currents with frequencies of 6 Hz and 8 Hz were applied to the prototype clutch. The output torque was estimated based on the trained neural network using internal magnetic field measurements. The actual transmitted

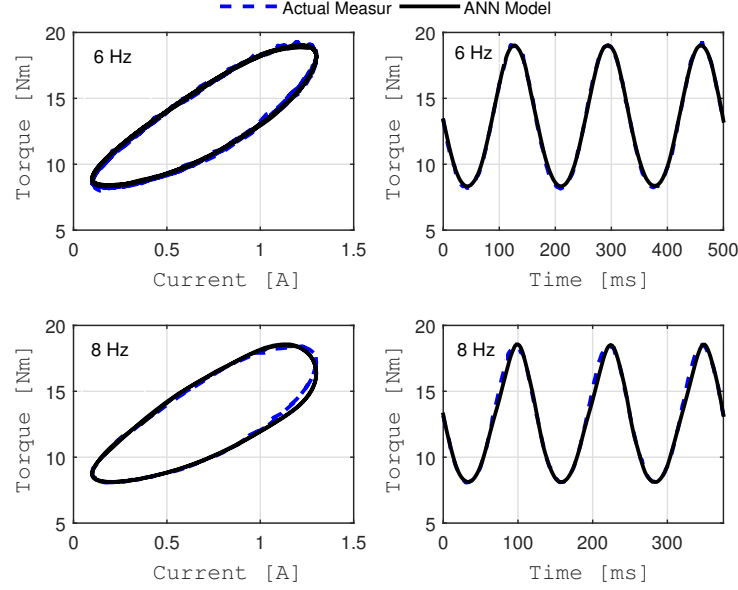


Figure 4.9: Actual torque measurements versus estimations.

torque was recorded via a load cell on the output shaft of the prototype clutch. Fig. 4.9 compares the predicted values of the output torque using the proposed neural network with those obtained experimentally using the load cell. The figure shows the estimated torque versus applied current (first column) as well as estimated and actual torque as functions of time (second column). The results show close match between the actual and predicted output torques despite the presence of heavy hysteresis in the HMR clutch.

#### 4.4.3 Torque Control

In this section, the performance of the proposed “sensor-less” force/torque tracking control scheme is presented. In the proposed scheme, the ANN provides the feedback signal for the PID controller that controls the output torque of the actuator. It should be noted that no other feedback signal, except for the embedded Hall sensors inside the HMR clutch were used to achieve these results. The load cell was only used for evaluation purpose. The block diagram of the control system was shown in Fig. 4.7. The gains of the PID controller were tuned in each experiment to establish best tracking results.

Fig. 4.10 shows torque estimations along with actual torque measurements. The output torque of the MR clutch was controlled to track a sinusoidal trajectory with various frequencies

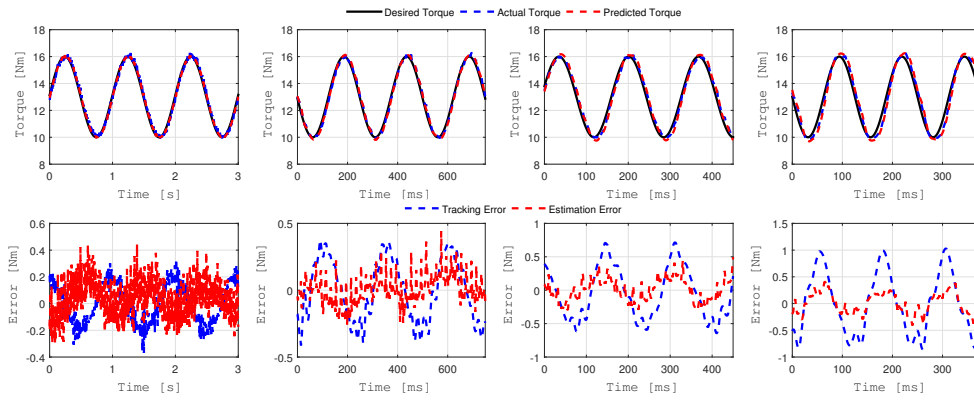


Figure 4.10: Torque control results for 1 Hz, 4 Hz, 6 Hz, and 8 Hz sinusoidal desired torque trajectories (from left to right).

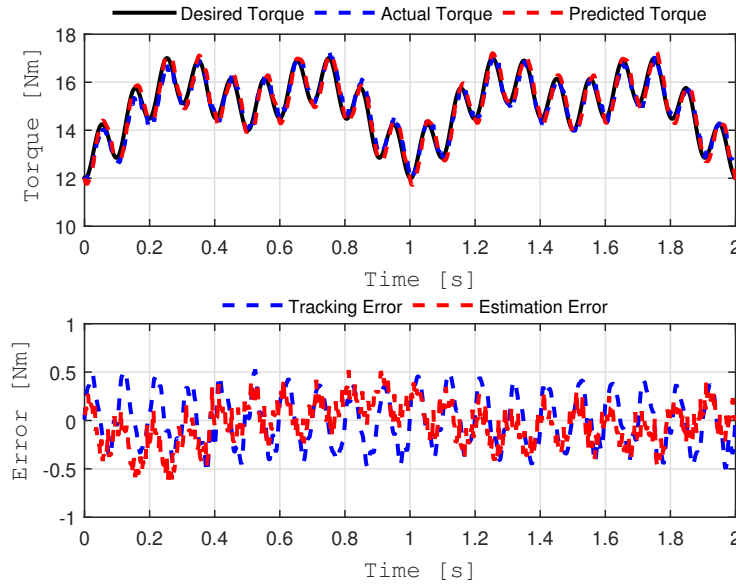


Figure 4.11: Torque control results for multi-sinusoidal reference signal.

ranging from 1 Hz to 8 Hz. This figure also includes both tracking and prediction errors for each desired input. The tracking error is computed as the difference between the estimated and the desired torque values, while the prediction error is the difference between the estimated and the actual torque measurement using the load cell.

In order to further evaluate the ability of the proposed approach, multi-sinusoidal<sup>1</sup> was used as the desired torque trajectories of the actuator. Fig. 4.11 demonstrates the results for the multi-sinusoidal desired torques along with tracking and prediction errors. As observed, there is a well agreement between the estimated output torque and those obtained using actual torque measurements. The results clearly show the capability of the proposed model to estimate the output torque and to perform torque tracking control where no external force/torque measurements are used in the control loop. These results validate the feasibility of “sensor-less” force/torque control scheme and suggest a cost-effective solution for torque control in human-safe robot applications using HMR clutches.

## 4.5 Conclusions and Future Works

MR clutches have been found to be a suitable for compliant actuation. In this regard, a new Hybrid MR clutch using a combination of a permanent magnet and an electromagnetic coil was designed and implemented. A modeling and control scheme using Artificial Neural Networks were proposed and studied. The performance of the prototype HMR clutch was then evaluated. The proposed modeling scheme became possible as a result of embedded Hall sensors inside the HMR clutch. The model was used to compensate for hysteresis between the input current and the output torque of the HMR clutch. This method eliminated the need for external force/torque sensors and provided a viable alternative to conventional force/torque control schemes. Experimental results verified the performance of the proposed modeling and control technique. Additional results for hybrid force and position control will be provided in our future work to further demonstrate clear advantages of this type of actuators for human-safe robotic applications.

---

<sup>1</sup> $T_d(t) = \sum_{i=1}^n A_i \cos(\omega_i t + \phi_i)$ , where  $A_i$ ,  $\omega_i$ , and  $\phi_i$ , for  $i = 1, \dots, n$  are the amplitude, frequency, and phase of each sinusoidal term, respectively.

# Bibliography

- [1] G. Pratt, M. M. Williamson, *et al.*, “Series elastic actuators,” in *Intelligent Robots and Systems 95. Human Robot Interaction and Cooperative Robots*, *Proceedings. 1995 IEEE/RSJ International Conference on*, vol. 1, pp. 399–406, IEEE, 1995.
- [2] M. Zinn, B. Roth, O. Khatib, and J. K. Salisbury, “A new actuation approach for human friendly robot design,” *The international journal of robotics research*, vol. 23, no. 4-5, pp. 379–398, 2004.
- [3] M. Kermani and A. Shafer, “Magneto-and electro-rheological based actuators for human friendly manipulators,” Sept. 30 2014. US Patent App. 14/502,389.
- [4] A. S. Shafer and M. R. Kermani, “On the feasibility and suitability of mr fluid clutches in human-friendly manipulators,” *Mechatronics, IEEE/ASME Transactions on*, vol. 16, no. 6, pp. 1073–1082, 2011.
- [5] M. R. Jolly, J. W. Bender, and J. D. Carlson, “Properties and applications of commercial magnetorheological fluids,” in *5th Annual International Symposium on Smart Structures and Materials*, pp. 262–275, International Society for Optics and Photonics, 1998.
- [6] J. D. Carlson and M. R. Jolly, “Mr fluid, foam and elastomer devices,” *mechatronics*, vol. 10, no. 4, pp. 555–569, 2000.
- [7] X. Wang and F. Gordaninejad, “Flow analysis of field-controllable, electro-and magneto-rheological fluids using herschel-bulkley model,” *Journal of Intelligent Material Systems and Structures*, vol. 10, no. 8, pp. 601–608, 1999.
- [8] B. Spencer Jr, S. Dyke, M. Sain, and J. Carlson, “Phenomenological model for magnetorheological dampers,” *Journal of engineering mechanics*, 1997.

- [9] A. Adly, I. Mayergoyz, and A. Bergqvist, "Preisach modeling of magnetostrictive hysteresis," *Journal of Applied Physics*, vol. 69, no. 8, pp. 5777–5779, 1991.
- [10] A. Visintin, *Differential models of hysteresis*, vol. 111. Springer Science & Business Media, 2013.
- [11] M. A. Krasnosel'Skii and A. V. Pokrovskii, *Systems with hysteresis*. Springer Science & Business Media, 2012.
- [12] P. Yadmellat and M. R. Kermani, "Adaptive modeling of a magnetorheological clutch," *Mechatronics, IEEE/ASME Transactions on*, vol. 19, no. 5, pp. 1716–1723, 2014.
- [13] K. D. Weiss and J. D. Carlson, "A growing attraction to magnetic fluids," *Machine design*, vol. 66, no. 15, pp. 61–64, 1994.
- [14] M. Moghani and M. R. Kermani, "Design and development of a hybrid magnetorheological clutch for safe robotic applications," in *Robotics and Automation (ICRA), 2016 IEEE International Conference on*, IEEE, 2016.
- [15] "Sent - single edge nibble transmission for automotive applications."
- [16] P. Yadmellat, A. S. Shafer, and M. R. Kermani, "Design and development of a safe robot manipulator using a new actuation concept," in *Robotics and Automation (ICRA), 2013 IEEE International Conference on*, pp. 337–342, IEEE, 2013.
- [17] W. T. Miller, P. J. Werbos, and R. S. Sutton, *Neural networks for control*. MIT press, 1995.
- [18] X. Dong, M. Yu, Z. Li, C. Liao, and W. Chen, "Neural network compensation of semi-active control for magneto-rheological suspension with time delay uncertainty," *Smart Materials and Structures*, vol. 18, no. 1, p. 015014, 2009.
- [19] C. Natale, F. Velardi, and C. Visone, "Identification and compensation of preisach hysteresis models for magnetostrictive actuators," *Physica B: Condensed Matter*, vol. 306, no. 1, pp. 161–165, 2001.
- [20] X. Zhang, Y. Tan, and M. Su, "Modeling of hysteresis in piezoelectric actuators using neural networks," *Mechanical Systems and Signal Processing*, vol. 23, no. 8, pp. 2699–2711, 2009.

- [21] R. Dong, Y. Tan, H. Chen, and Y. Xie, “A neural networks based model for rate-dependent hysteresis for piezoceramic actuators,” *Sensors and Actuators A: Physical*, vol. 143, no. 2, pp. 370–376, 2008.
- [22] D. R. Seidl, S.-L. Lam, J. Putman, R. D. Lorenz, *et al.*, “Neural network compensation of gear backlash hysteresis in position-controlled mechanisms,” *Industry Applications, IEEE Transactions on*, vol. 31, no. 6, pp. 1475–1483, 1995.
- [23] K. Gurney, *An introduction to neural networks*. CRC press, 1997.

# **Chapter 5**

## **Conclusions and Future Work**

### **5.1 Conclusion**

In this work, a new magnetic actuation mechanism inside Magneto-Rheological actuators was presented. The novel design takes benefit from the combination of the electromagnetic coil and permanent magnet. Finite Element Analysis was hired to fully study the characteristic of the new design. The location of the permanent magnet was chosen carefully in the optimal design of the MR clutch. The newly designed MR clutch was then manufactured to be investigated and compared to its coil based counterpart. The optimal light-weight design of the HMR clutches and inherently back-drivable nature of these devices make them an ideal candidate for human-safe robotic applications.



## 5.2 Future Work

### 5.2.1 Validating Antagonistic DASA using HMR and Conventional MR clutches

The designed test bench has the capacity to be equipped with two MR clutches. In order to study the A-DASA approach, a previously built conventional MR clutch should be mounted on the test bench. A-DASA was validated by integrating two clutches that share the same characteristic [1, 2]. However, this approach can be extended using HMR clutch and its counterpart using electromagnetic coil. Antagonistic-DASA Experimentation Platform is shown in Fig. 5.1.

### 5.2.2 Hybrid Motion-Force Control

Safe interaction with the environment requires the robotic manipulator to control motions and forces while the manipulator is in contact with a rigid environment. Hybrid motion-force control exploits both control signals produced by two independent motion and force controllers in which motions and forces should be independently controlled. Here, the use of Hall sensors inside the clutch provides obligatory information to compensate the hysteretic relationship between the input current and output torque of the clutch. Using the developed neural network and measuring the internal magnetic field, cost effective “sensorless” torque control can be achieved. Position data can be acquired from an encoder which monitors the output shaft.

### 5.2.3 Multi-DOF Light Weight Manipulator

This work can be integrated in the construction of a multi-DOF manipulator or a robotic exoskeleton implementing the A-DASA approach. Permanent magnet introduces “Fail-safe” feature into DASA approach. Fail-safe feature is one that, allows the robotic manipulator to maintains its position in the event of unintended interruption of the electrical input power. The construction of a multi-DOF manipulator can take benefits from the fail-safe feature of HMR clutches. A conceptual design of a light-weight robotic exoskeleton using HMR clutch is depicted in Fig. 5.2. A single motor drives the input to two sets of HMR clutches, in opposite directions with respect to one another. The antagonistic output of each sets of clutches are coupled to the first and second joint of the shoulder, respectively. This design results in low inertia,

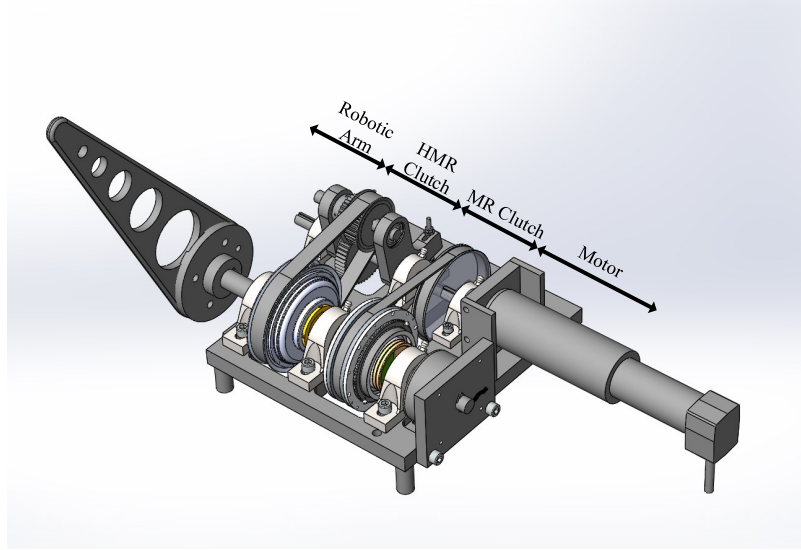


Figure 5.1: A-DASA Experimentation Platform.

controllable stiffness, and back-drivable transmissions with zero backlash for shoulder's joint.

#### 5.2.4 Redesign the Location of the Hall Sensors

The current design is formed by embedding the Hall sensor inside the sandwich pack of two steel and one aluminum disk. The selection of aluminum disk was the result of the previous study to provide a non-hysteretic environment to Hall sensors and makes the reading clear. However, the low permeability of the aluminum disk creates huge air gap in the magnetic circuit in comparison to the other parts and sacrifices the performance of the MR clutch. On the other hand, the sandwich pack of two steel and one aluminum disk increases the total height of the clutch, ergo increasing the total mass of actuator. Moreover, integrating the Hall sensor in the middle of clutch pack rises manufacturing and assembling issues.

For future work, the sandwich pack assembly can be replaced by a non-magnetic disk with built-in Hall sensor. A simulation is performed to validate this concept. Fig. 5.3 illustrates a computer simulation regarding the new place of the Hall sensors. As seen, the magnetic path is perpendicular to the flat surface of the Hall sensor.

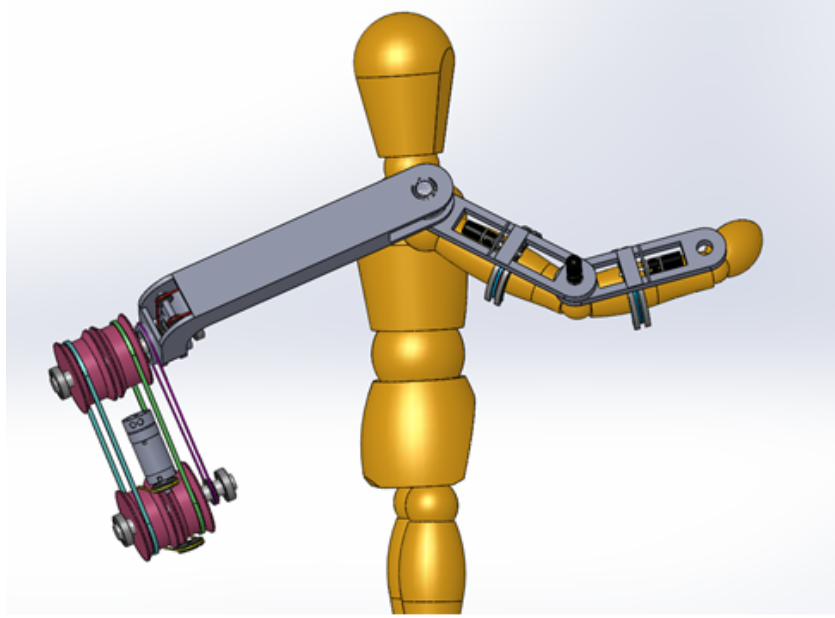
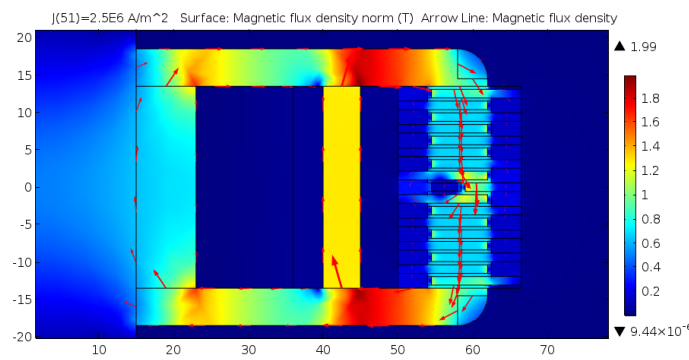
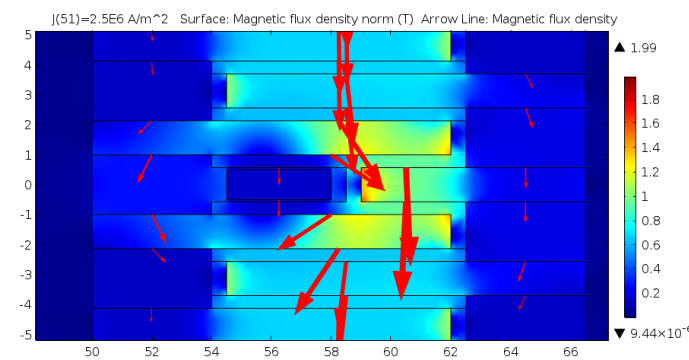


Figure 5.2: Conceptual design of a light-weight robotic exoskeleton.



(a)



(b)

Figure 5.3: (a)Magnetic flux density contour map. (b)The path of the magnetic field is perpendicular to the surface of the Hall sensor.

# Bibliography

- [1] P. Yadmellat, A. S. Shafer, and M. R. Kermani, “Design and development of a single-motor, two-dof, safe manipulator,” *Mechatronics, IEEE/ASME Transactions on*, vol. 19, no. 4, pp. 1384–1391, 2014.
- [2] A. S. Shafer and M. R. Kermani, “Development of high performance intrinsically safe 3-dof robot,” in *Robotics and Automation (ICRA), 2014 IEEE International Conference on*, pp. 619–624, IEEE, 2014.

# Curriculum Vitae

**Name:** Masoud Moghani

**Post-Secondary Education and** Western University  
London, ON, Canada

**Degrees:** 2014 - 2016 M.E.Sc.  
Electrical and Computer Engineering Department, Robotics and Control

K. N. Toosi University of Technology (KNTU)  
Tehran, Iran  
2009 - 2013 B.E.Sc.  
Mechanical Engineering Department

**Honours and Awards:** Western Graduate Research Scholarship  
Western University  
2014 - 2016

Graduated with distinction from Mechanical Engineering Department  
K. N. Toosi University of Technology  
2013

**Related Work Experience:** Research and Teaching Assistant  
Western University  
2014 - 2016

**Publications:**

- **Moghani M.**, Kermani, M. R., “Design and Development of a Hybrid Magneto-Rheological Clutch for Safe Robotic Applications,” In 2016 IEEE International Conference on Robotics and Automation (ICRA) (pp. 3083-3088). IEEE.
- **Moghani M.**, Kermani M. R., “Hysteresis Modeling of a Hybrid Magneto- Rheological Actuator,” to appear: IEEE International Conference on Advanced Intelligent Mechatronics